論文 / 著書情報
Article / Book Information

題目(和文)	低質量な複数の衛星からなる衛星系の形成
Title(English)	Formation of low-mass multiple satellites
著者(和文)	武田隆顕
Author(English)	
出典(和文)	学位:博士(理学), 学位授与機関:東京工業大学, 報告番号:甲第4983号, 授与年月日:2002年3月26日, 学位の種別:課程博士, 審査員:
Citation(English)	Degree:Doctor (Science), Conferring organization: Tokyo Institute of Technology, Report number:甲第4983号, Conferred date:2002/3/26, Degree Type:Course doctor, Examiner:
学位種別(和文)	博士論文
Type(English)	Doctoral Thesis

Formation of Low-Mass Multiple Satellites

Takaaki Takeda

Department of Earth and Planetary Sciences,
Tokyo Institute of Technology

March 2002

ABSTRACT

We have investigated the evolution of a circumplanetary disk and accretion of satellite(s) from the disk by N-body simulations. As for formation of the Moon, it is considered that a giant impact between rocky planets (terrestrial planets) generate a debris disk, and the Moon is accreted from the disk. Satellites around a gas giant planet are also considered to be formed from a disk around the planet, and satellites and rings are by-products of planet formation. Several senarios had been considered as the origin of a proto-satellite disk. In this paper, we investigate satellite accretion process from a disk which is initially distributed within Roche limit. Radial redistribution of the disk mass is important for the process. We consider not only a massive disk relative to mass of a host planet, which results in a large single satellite such as the Moon, but also a less massive disk that produces low mass multiple satellites. We derived the condition of an initial disk for formation of multiple satellites. Through semi-analytical arguments and N-body simulations, we find the mass of a primary satellite as a function of initial disk parameters (disk mass $M^0_{\rm disk}$ and specific angular momentum $l^0_{\rm disk}$). The mass of the satellite $M_{\rm s}$ is regulated by the balance between viscous spreading of the disk and disk-satellite interaction. When the satellite grows enough, it opens a gap between the disk and itself, to halt its growth. In the case that $M_{\rm s}/M_{\rm disk} \gtrsim 1$, where $M_{\rm disk}$ is the mass of the remaining disk, disk-satellite interaction clears the disk, and a single satellite remains. In the case that $M_{\rm s}/M_{\rm disk} \ll 1$, the disk repels a primary satellite outward, and extends beyond Roche limit to form a next satellite. Since we find that $M_{\rm s} \propto (M^0_{\rm disk}/M_{\rm c})^2$, where $M_{\rm c}$ is the mass of the host planet, a less massive disk leads to multiple satellites. The condition for formation of a secondary satellite depends on $M^0_{\rm disk}$ and $l^0_{\rm disk}$. From a debris disk with $l^0_{\rm disk} \sim 0.8\sqrt{GM_{\rm c}R_R}$, where $R_{\rm R}$ is the Roche radius, a single satellite would be formed if $M^0_{\rm disk} \gtrsim 0.03M_{\rm c}$, while two or more satellites would be formed if $M^0_{\rm disk} \lesssim 0.03M_{\rm c}$. When a two-satellite system is formed, these satellites are locked in the 2:1 orbital resonance in our simulation range. Extrapolating the above results to further less massive disks, we find that satellite system similar to the Galilean satellites of Jupiter (4-5 satellites with mass $M_{\rm s} \sim 10^{-4}$-$10^{-5}M_{\rm c}$) may be formed from a disk with $M^0_{\rm disk} \sim 0.003M_{\rm c}$. The diversity of satellite systems in the solar system may come from the different initial circumplanetary disks relative to the host planet's mass.

Contents

1. INTRODUCTION

Most of the planets in the solar system have satellite systems around them. A satellite system with relatively high mass ratio compared to the central planet, such as Earth/Moon system ($M_s/M_c \sim 0.012$, where M_s and M_c are mass of a satellite and a central planet) or Pluto/Charon system ($M_s/M_c \sim 0.1$), has only one satellite. On the other hand, a gaseous planet has multiple satellites. A satellite system with multiple satellites has small mass ratio compared to the host planet. We show masses and orbital radii of satellites of gaseous planets in Figs. 1. The horizontal and vertical axes are orbital radii and masses of satellites, which are normalized by the radius and mass of each host planet R_c and M_c. Panels (a)-(d) are for Jupiter, Saturn, Uranus, and Neptune respectively. In general, gaseous planets have several satellites with substantial mass $M_s/M_c \sim 10^{-4}$-10^{-5} in a region from 5 to 30 R_c. One exception is Neptune. It is often considered that the satellites of Neptune is lost by a capture of Triton. Near the host planet, many small satellites exist, and the inner satellite has the smaller mass in general.

The satellites mentioned above have prograde orbit and low inclination. In the cases of gaseous planets, they are called regular satellites. In general, it is considered that regular satellites are accreted from a circumplanetary disks. Diversity of satellite systems would come from diversity of proto-satellite disk. About origin of satellite systems, one question is that how significant amount of material is emplaced in orbit around a protoplanet, and another question is how a satellite system with suitable mass and number of satellites is formed from the proto-satellite disk. In this paper, we concentrate on a dynamical aspect of satellite accretion process from proto-satellite disk, expanding a method of N-body simulations for a massive satellite formation process (Ida, Canup & Stewart 1997) to a less massive region.

As for an origin of the proto-satellite disk, following four models are considered (e.g. Lunine & Tittemore 1993, Pollack, Lunine, & Tittemore 1991, Stevenson, Harris, & Lunine 1986).

(a) Accretion disk: A gaseous giant planet grows by rapid gas accretion of proto-

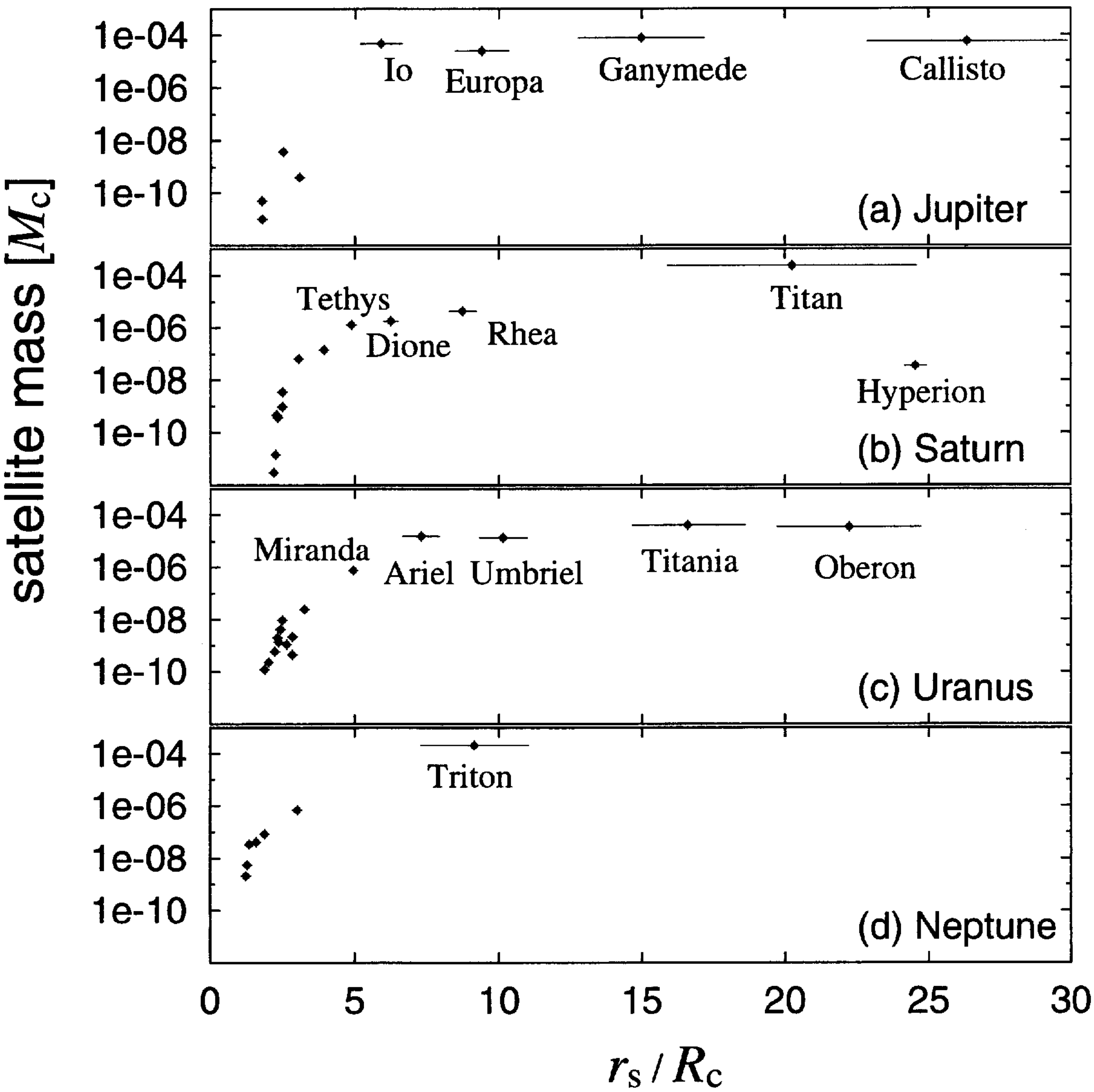

Fig. 1.— Masses and orbital radii of satellites of gaseous planets. The horizontal and vertical axes are orbital radii and mass of satellites, which are normalized by the radius and mass of each host planet (R_c and M_c). Masses of smallest satellites of outer planets are not yer determined exactly. In this figures, we estimated the masses of satellites by their observed sizes. Horizontal bar represents $5r_H$ of each satellite.

planetary nebula after a core grows massive enough. Mixture of gas and dust flows into the Hill's sphere of the planet, and this can form an accretion disk about the protoplanet.

(b) Spin-out disk: Initially, a radius of a gas giant planet is much larger than the present radius. As the inflow from the protoplanetary nebula slows down, the planet contracts, and material of the envelope is left behind in a form of a disk.

(c) Blow-out disk: A giant impact can blow out material of the impactor and the target to the orbit about the protoplanet.

(d) Co-accretion disk: Collisions of planetesimals within the Hill's sphere of the protoplanet will generate a debris disk about the protoplanet.

Since model (d) predicts a disk whose size is comparable to the Hill's sphere of the planet, which is orders of magnitude larger than the extent of observed regular satellites, it may be excluded (Pollack, Lunine, & Tittemore 1991). Models (a) and (b) are often considered as the origin of the proto-satellite disks of gaseous planets. In the case of lunar origin, model (c) is most favored (Hartmann & Davis 1975; Cameron & Ward 1976), and this model is also compelling for Uranus, whose axial tilt is considered to be an outcome of a giant impact. However, there is no consensus of the origin and the properties of a proto-satellite disk.

In this paper, we concentrate on the accretional process of satellite(s) from a proto-satellite disk. We perform N-body simulations and investigate the evolution of a disk which is initially within the Roche limit. This is a limit of a radially compact disk. In such a system, redistributions of mass and angular momentum of the disk are important. In a context of lunar origin, N-body simulations showed that a single large satellite such as the Moon is formed from a radially compact and relatively heavy disk (Ida, Canup & Stewart 1997). We will expand this work to a less massive region, and show that a multiple satellite system is formed from a less massive disk. The difference between a system with a single massive satellite and that with multiple small satellites comes from the difference of the initial condition of a proto-satellite disk. The evolution of a less massive disk has not been studied in previous N-body simulations about lunar formation. This is because particle number needed to properly express the debris disk increases with decreasing disk mass (see section 2.4.2). Moreover, the time scale of disk evolution increases with decreasing disk mass. We performed N-body simulations with large number of particles (initial $N = 10^5$), using GRAPE-5 system (Kawai, Fukushige, Makino & Taiji 2000) for calculations of mutual gravity. We found that in a case that initial disk mass is relatively small, a secondary satellite is formed from a residual disk after a primary satellite is formed. In our parameter range of the simulations, the secondary satellite has smaller mass than the primary satellite by a factor 0.3-0.6, and the satellite orbits are locked in 2:1 resonance.

Here, we briefly summarize the accretional process of satellite(s). In the case of lunar formation, it is considered that a giant impact between the proto-Earth and a Mars-sized planetesimal generated a debris disk around the proto-Earth (Hartmann & Davis 1975; Cameron & Ward 1976), with most of its mass within the Roche limit. The accretion from an impact generated massive disk is also a strong candidate for the origin of Charon, which is the satellite of Pluto and has larger satellite-planet mass ratio (~ 0.1) than Earth-Moon system (~ 0.012)(Kokubo, Ida & Makino 2000). The disks for Moon and Charon would initially have mass a few times as massive of them: $M^0_{\rm disk} \sim 0.02$-$0.04 M_{\rm c}$ for Moon and 0.2-0.4 $M_{\rm c}$ for Charon, where $M^0_{\rm disk}$ is the mass of an initial disk. In an optically thick debris disk, which is within the Roche limit, the gravitational instability leads to development of trailing spiral structure, which carries angular momentum outward. The development of spiral structure is a common feature of an optically thick debris disk, from a massive protolunar disk to a much less massive planetary ring such as Saturnian ring (Salo 1995; Daisaka & Ida 1999). With the angular momentum transfer, the disk spreads radially, and materials diffuse out from the Roche limit. Angular momentum transfer rate depends on surface density of the disk, and the time scale of diffusion of such a massive disk as a protolunar disk is as short as 1 month (Kokubo, Ida & Makino 2000; Takeda & Ida 2001). A satellite forms outside the Roche limit with the materials transfered outside the Roche limit. The reason why a single large satellite is formed is that a satellite seed just outside the Roche limit grows preferentially, fed by the mass diffused out from the disk. In the simulations of lunar formation, most of the material in the initial disk is consumed for lunar formation or falls to the Earth.

However, as shown in following sections, multiple satellite system is formed from a less massive disk. The formation of a two satellite system is as follows. As the satellite mass increases and disk mass diminishes, the satellite forms a gap between the disk and itself, and the growth of the satellite stops. This mechanism is an analogue to the gap formation of Jovian planets in protoplanetary nebula or shepherding of the ring by a satellite in Saturnian ring (Lin & Pringle 1993; Goldreich & Tremaine 1980). Thus, the satellite mass has an upper limit. After the gap is formed, tidal torque between the disk and a satellite carries angular momentum from the disk to the satellite (e.g., Lin & Pringle 1993). Through the interaction, the satellite gains angular momentum from the disk and migrates outward, while the disk loses angular momentum. The outcome depends on the mass of the satellite and the mass of the remaining disk. If the satellite is massive comparing with the remaining disk, the disk falls to the central planet. In this case, final outcome is a single satellite system (Ida, Canup & Stewart 1997; Kokubo, Ida & Makino 2000). In the case that the satellite mass is small compared with the remaining disk, the satellite migrates well beyond the Roche limit. Then, disk mass spreads beyond the Roche limit again, and the disk spawns a secondary satellite near the Roche limit. The orbits of two satellite formed in this way are in 2:1 resonance in most runs of our simulations. This comes from the resonance interactions between a satellite and the disk (Goldreich & Tremaine 1978).

In this paper, we investigate the mass and number of satellites which are formed from a proto-satellite disk, expanding the theory of satellite formation from a massive debris disk for the lunar formation in Ida, Canup & Stewart (1997) and Kokubo, Ida & Makino (2000) to a less massive disk. Especially, we derive a criterion between the single satellite system formation and the two-satellite system formation. We perform N-body simulations and show that a multiple satellite system is formed from a debris disk with $M_{\rm disk}^0 \lesssim 0.03 M_{\rm c}$ We predict number and masses of the satellites as functions of initial mass $M_{\rm disk}^0$ and specific angular momentum $l_{\rm disk}^0$ of the disk. Satellites which resemble Galilean satellites of Jupiter are formed from a disk which has mass of 0.3 % of Jupiter.

In discussion, we apply the result to formation of multiple satellite system like Galilean satellite system.

In section 2, we describe angular momentum transfer processes in the disk, and summarize the properties of angular momentum transfer. In section 3, we describe the method of numerical simulations. In section 4, we first show overview of viscous evolution of a disk, and we describe gap formation, and investigate the relation between mass of a satellite and the remaining disk when the growth of the satellite stops. In section 5, we describe formation of a secondary satellite and derive the criterion for formation of two-satellite system, and compare them with the results of N-body simulations. In section 6, we discuss the relations between a satellite and an initial proto-satellite disk, extending the results to a further less massive disk, and compare them with the satellite system of the solar system. This would give a clue for the diversity of satellite systems.

2. VISCOUS EVOLUTION OF THE DISK

2.1. Viscous Spreading of the Disk and Accretion of a Satellite

We investigate the evolution of a radially compact disk, which is initially confined within the Roche limit. Roche limit is a limit within which the tidal force of the central planet is stronger than the self gravity of an orbiting body. Within the Roche limit, an aggregate of particles is sheared apart by tidal effect. Thus, no satellite can be formed within the Roche limit. However, the disk radially spreads, and satellite accretion occurs outside the Roche limit eventually. Once a satellite is formed outside the Roche limit, the satellite grows with mass spreaded out beyond the Roche limit, until the gravity of the satellite forms a gap between the disk and itself. The gap formation is regulated by balance between spreading of the disk and satellite-disk interaction. Thus, viscous evolution of the disk is essential for satellite formation process. In this section, we describe viscous spreading of a particulate disk within the Roche limit.

2.1.1. Roche limit

The radius of the Roche limit is given as

$$R_{\rm R} = 2.456 \left(\frac{\rho}{\rho_{\rm c}}\right)^{-1/3} R_{\rm c}, \tag{1}$$

where ρ, $\rho_{\rm c}$ and $R_{\rm c}$ are a mass density of the disk material, a mass density of the central planet and a radius of the central planet. The width of a region $[R_{\rm c}\text{-}R_{\rm R}]$ depends on the ratio of the mass density of the disk material and the central planet. Note that the Roche radius is a radius of the Roche limit, and not a radius of the Roche lobe. Roche lobe denotes a region within which the gravity of the planet dominates over the gravity of the sun and the centrifugal force of the rotation around the sun. The radius of the Roche limit is a few $R_{\rm c}$, while the radius of Roche lobe is orders of magnitudes larger.

In the case of a lunar formation, $\rho_{\rm c} = 5.5$ g cm^{-3}, and $\rho = 3.3$ g cm^{-3}, which are the present Earth's and lunar bulk densities, so that $R_{\rm R} = 2.9 R_{\rm c}$, or $R_{\rm c} = 0.34 R_{\rm R}$. In our simulations, we adopt the relation $R_{\rm c} = 0.34 R_{\rm R}$, because a comparison with the

N-body simulations of lunar formation is easier. However, multiple satellite systems are common in outer solar system, so that we mention Jovian and Saturnian system briefly here. Assuming that particles are of mixture of rock and ice with $\rho \sim 2$, which is about a material density of Ganymede, the radius of Jupiter is $R_{\rm J} \sim 0.45 R_{\rm R}$, and assuming that $\rho \sim 1.5$, which is about a material density of Dione, the radius of Saturn is $R_{\rm S} \sim 0.53 R_{\rm R}$. In outer solar system, the region $R_{\rm c} < r < R_{\rm R}$ is narrower than the terrestrial case. However, since outer edge of a disk is more important in the satellite formation process, the result of this paper can be appliable to outer solar system with small modifications.

2.1.2. Angular momentum transfer and viscous spreading

The spreading of a disk is regulated by angular momentum transfer. If angular momentum is transfered outward, inner material loses angular momentum and migrates inward, while outer material gains angular momentum and migrates outward (Lynden-bell & Pringle 1974). Thus, the spreading of a disk can be described by outward angular momentum transfer. In sections 2.2 and 2.3, we summarize angular momentum transfer processes in a self-gravitating particulate disk, and derivation of these angular momentum transfer rates in our numerical simulations, following Takeda & Ida (2001). In section 2.4, we show the properties of angular momentum transfer.

2.2. Basic Equations of Angular Momentum Transfer

Number density distribution function $f(\boldsymbol{x}, \boldsymbol{v}, m)$ satisfies the Boltzmann equation, where $\boldsymbol{x}$,$\boldsymbol{v}$, and m denote position, velocity and mass of particles, respectively:

$$\frac{\partial f}{\partial t} + v_\alpha \frac{\partial f}{\partial x_\alpha} - \frac{\partial \Phi}{\partial x_\alpha} \frac{\partial f}{\partial v_\alpha} = \left(\frac{\partial f}{\partial t}\right)_c + \left(\frac{\partial f}{\partial t}\right)_g, \tag{2}$$

where the derivatives with suffix $(\partial X/\partial t)_c$ and $(\partial X/\partial t)_g$ mean that the change of a quantity X is due to mutual collisions and gravitational interactions. Φ is the external potential from the central planet. We multiply eq. (2) by m and integrating it over m.

Since $\partial\Phi/\partial x_\alpha$ does not depend on m, an equation for mass density g is

$$\frac{\partial g}{\partial t} + v_\alpha \frac{\partial g}{\partial x_\alpha} - \frac{\partial \Phi}{\partial x_\alpha}\frac{\partial g}{\partial v_\alpha} = \left(\frac{\partial g}{\partial t}\right)_c + \left(\frac{\partial g}{\partial t}\right)_g, \tag{3}$$

where $g(\boldsymbol{x}, \boldsymbol{v}) \equiv \int mf dm$. In this paper, we will simulate an equal-mass ($m_{\rm p}$) system, then $g = m_{\rm p} f$.

We integrate eq. (3) in cylindrical coordinates over z, θ and $\boldsymbol{v}$. After some partial integrations, we obtain the equation of continuity:

$$\frac{\partial}{\partial t}(2\pi\Sigma) + \frac{1}{r}\frac{\partial}{\partial r}(2\pi r\Sigma u_r) = \left(\frac{\partial}{\partial t}2\pi\Sigma\right)_c + \left(\frac{\partial}{\partial t}2\pi\Sigma\right)_g, \tag{4}$$

where $\Sigma(r,t)$ and $\boldsymbol{u}(r,t)$ are surface mass density and averaged velocity defined by

$$\Sigma(r,t) \equiv \frac{1}{2\pi}\int_0^{2\pi} d\theta \int_{-\infty}^{\infty} dz \int d\boldsymbol{v} g, \tag{5}$$

$$\Sigma\boldsymbol{u}(r,t) \equiv \frac{1}{2\pi}\int_0^{2\pi} d\theta \int_{-\infty}^{\infty} dz \int d\boldsymbol{v}\boldsymbol{v} g. \tag{6}$$

Since collision and gravitational force do not change the location of particles discontinuously, the right hand side of eq. (4) is 0.

Similarly, eq. (3) multiplied by v_θ with integrations over z, θ and $\boldsymbol{v}$ leads to the θ component of equation of motion,

$$\frac{\partial}{\partial t}(2\pi\Sigma u_\theta) + \frac{1}{r^2}\frac{\partial}{\partial r}\left(r^2\int_0^{2\pi} d\theta \int_{-\infty}^{\infty} dz \int d\boldsymbol{v} v_r v_\theta g\right) = \left(\frac{\partial}{\partial t}2\pi\Sigma u_\theta\right)_c + \left(\frac{\partial}{\partial t}2\pi\Sigma u_\theta\right)_g. \tag{7}$$

Multiplying eq. (7) by r^2, we obtain the equation of angular momentum,

$$\frac{\partial}{\partial t}(2\pi r\Sigma r u_\theta) = -\frac{\partial F_{\rm AM}}{\partial r}, \tag{8}$$

where

$$F_{\rm AM} = F_{\rm trans} + F_{\rm col} + F_{\rm grav} + \dot{M}_{\rm disk} h \tag{9}$$

$$F_{\rm trans} \equiv \int_0^{2\pi} r d\theta \int_{-\infty}^{\infty} dz \int d\boldsymbol{v} v_r r v_\theta g - \dot{M}_{\rm disk} h, \tag{10}$$

$$F_{\rm col} \equiv -\int_{r_{\rm min}}^{r} dr' \left(\frac{\partial}{\partial t}2\pi r'\Sigma r' u_\theta\right)_c, \tag{11}$$

$$F_{\rm grav} \equiv - \int_{r_{\rm min}}^{r} dr' \left(\frac{\partial}{\partial t} 2\pi r' \Sigma r' u_\theta \right)_g . \tag{12}$$

We introduced specific angular momentum $h \equiv r u_\theta$ and advective term $\dot{M}_{\rm disk} \equiv 2\pi r \Sigma u_{\rm r}$, which expresses angular momentum carried by mean radial flow. Since $F_{\rm AM}$ appears in eq. (8) as the form $\partial F_{\rm AM}/\partial r$, the minimum range of integration $r_{\rm min}$ is a free parameter. We choose $r_{\rm min}$ as the radius of inner boundary of the disk, so that $F_{\rm col}$ and $F_{\rm grav}$ are 0 inside of inner boundary and outside of outer boundary of the disk. Since $\dot{M}_{\rm disk} = 2\pi r \Sigma u_r = \int_0^{2\pi} r d\theta \int_{-\infty}^{\infty} dz \int d\boldsymbol{v} u_r r u_\theta g$,

$$F_{\rm trans} = \int_0^{2\pi} r d\theta \int_{-\infty}^{\infty} dz \int d\boldsymbol{v} (v_r - u_r) r (v_\theta - u_\theta) g. \tag{13}$$

This term is angular momentum transfer due to random motion of particles, analogous to that due to molecular viscosity (Goldreich & Tremaine 1978). Wisdom & Tremaine (1988) and Araki & Tremaine (1986) called it "local" and "translational" transfer, respectively. We will call this flux as "translational" angular momentum flux and use suffix "trans".

Combining eq. (4) and eq. (8),

$$\dot{M}_{\rm disk} \frac{\partial h}{\partial r} = -2\pi r \Sigma \frac{\partial h}{\partial t} - \frac{\partial}{\partial r} \left(F_{\rm trans} + F_{\rm col} + F_{\rm grav} \right). \tag{14}$$

As long as $M_{\rm disk} \ll M_{\rm c}$, u_θ is Keplerian, $u_\theta = r\Omega = \sqrt{GM_{\rm c}/r}$, and $\partial h/\partial t = 0$. Then

$$\dot{M}_{\rm disk} = - \frac{1}{\partial h/\partial r} \frac{\partial}{\partial r} \left(F_{\rm trans} + F_{\rm col} + F_{\rm grav} \right), \tag{15}$$

where $\partial h/\partial r = \Omega r/2$.

Angular momentum transfer is often expressed in terms of viscosity ν (e.g. Lynden-bell & Pringle 1974; Pringle 1981). In a viscous accretion disk,

$$\dot{M}_{\rm disk} = -3\pi \left(\Sigma\nu + 2r \frac{\partial \Sigma \nu}{\partial r} \right), \tag{16}$$

$$F_{\rm AM} = \dot{M}_{\rm disk} h + 3\pi r^2 \Sigma \Omega \nu. \tag{17}$$

Comparing eqs. (9) and (15) with eqs. (16) and (17), effective viscosity ν is given by

$$3\pi \Sigma r^2 \Omega \nu = F_{\rm trans} + F_{\rm col} + F_{\rm grav}. \tag{18}$$

2.3. Derivation of Angular Momentum Transfer Rates in Numerical Simulation

In this subsection, we derive expressions of F_{trans}, F_{col} and F_{grav} in a particle disk, generalizing the procedure in Wisdom & Tremaine (1988). Particle i is represented as $\delta(\boldsymbol{x}-\boldsymbol{x}_i)\delta(\boldsymbol{v}-\boldsymbol{v}_i)\delta(m-m_i)$ in phase space $(\boldsymbol{x},\boldsymbol{v},m)$, where $\boldsymbol{x}_i$, $\boldsymbol{v}_i$ and m_i are the position of mass, velocity and mass of particle i, and δ is delta function. Mass density distribution $g(\boldsymbol{x},\boldsymbol{v})$ is

$$g = \int dmf = \sum_i m_i\delta(\boldsymbol{x}-\boldsymbol{x}_i)\delta(\boldsymbol{v}-\boldsymbol{v}_i). \tag{19}$$

With eq. (19), we rewrite F_{local}, F_{col} and F_{grav} in particle image as below.

2.3.1. Translational angular momentum transfer

Substituting eq. (19) into eq. (13), we obtain

$$\begin{aligned} F_{\mathrm{trans}}(r) &= \int_0^{2\pi} rd\theta \int_{-\infty}^{\infty} dz \int d\boldsymbol{v}\,(v_r - u_r(r))\,r\,(v_\theta - u_\theta(r))\,g \\ &= \sum_i m_i(v_{ri}-u_r(r))r(v_{\theta i}-u_\theta(r))\delta(r-r_i). \end{aligned} \tag{20}$$

It is convenient to average F_{trans} over finite range $[r-\frac{1}{2}r_0, r+\frac{1}{2}r_0]$, where $r_{\mathrm{p}} \ll r_0 \ll r$ (r_{p}: particle physical radius). In our numerical simulation, we adopt $r_0 = 0.02R_{\mathrm{R}}$.

Averaged translational angular momentum transfer is

$$\begin{aligned} \overline{F_{\mathrm{trans}}}(r) &= \frac{1}{r_0}\int_{r-\frac{1}{2}r_0}^{r+\frac{1}{2}r_0} dr' F_{\mathrm{trans}}(r') \\ &= \frac{1}{r_0}\sum m_i(v_{ri}-u_{ri})r_i(v_{\theta i}-u_{\theta i}), \end{aligned} \tag{21}$$

where summation is taken in the region $r-\frac{1}{2}r_0 < r_i < r+\frac{1}{2}r_0$, and $\boldsymbol{u}_i$ is field velocity at $\boldsymbol{r}_i$.

We must define the averaged velocity $\boldsymbol{u}_i$. Substituting eq. (19) into eqs. (5), and (6), we obtain $\Sigma(r)$ and $\boldsymbol{u}(r)$ in particle image. We average them over r_0. The averaged surface density $\Sigma \equiv \overline{\Sigma}(r)$ and averaged velocity $\boldsymbol{u} \equiv \overline{\boldsymbol{u}}(r)$ are

$$\Sigma \equiv \frac{1}{2\pi r r_0} \int_{r-\frac{1}{2}r_0}^{r+\frac{1}{2}r_0} dr' \int_0^{2\pi} d\theta \int_{-\infty}^{\infty} dz \int d\boldsymbol{v} g = \frac{1}{2\pi r r_0} \sum_j m_j, \tag{22}$$

$$\boldsymbol{u} \equiv \frac{1}{2\pi r r_0 \Sigma} \int_{r_i-\frac{1}{2}r_0}^{r_i+\frac{1}{2}r_0} dr' \int_0^{2\pi} d\theta \int_{-\infty}^{\infty} dz \int d\boldsymbol{v} \boldsymbol{v} g = \frac{1}{2\pi r r_0 \Sigma} \sum_j \boldsymbol{v}_j m_j, \tag{23}$$

where the summations are taken over all particles in the range $[r - \frac{1}{2}r_0, r + \frac{1}{2}r_0]$.

2.3.2. Collisional angular momentum transfer

From equation (11),

$$F_{\rm col} = - \int_{r_{\rm min}}^{r} dr' \int_0^{2\pi} r' d\theta \int_{-\infty}^{\infty} dz \int d\boldsymbol{v} r' v_\theta \left(\frac{\partial g}{\partial t} \right)_{\rm c}. \tag{24}$$

Collision term $(\partial g/\partial t)_{\rm c}$ is the sum of the change of distribution function g over all collisions in a unit time. During a collision between particle A and B, the locations of the particles do not change, and the velocity of each particle changes as $\boldsymbol{v}_{\rm A} \to \boldsymbol{v}_{\rm A} + \Delta\boldsymbol{v}_{\rm A}$, $\boldsymbol{v}_{\rm B} \to \boldsymbol{v}_{\rm B} + \Delta\boldsymbol{v}_{\rm B}$ $(m_{\rm A}\Delta\boldsymbol{v}_{\rm A} + m_{\rm B}\Delta\boldsymbol{v}_{\rm B} = 0)$. Thus, $F_{\rm col}$ is

$$F_{\rm col} = - \sum_{\rm col} \int_{r_{\rm min}}^{r} dr' \{ m_{\rm A}\delta(r' - r_{\rm A})\Delta v_{\theta{\rm A}} + m_{\rm B}\delta(r' - r_{\rm B})\Delta v_{\theta{\rm B}} \} = - \sum_{\rm col} m_{\rm A} r_{\rm A} \Delta v_{\theta{\rm A}}, \tag{25}$$

where we assumed $r_{\rm A} < r_{\rm B}$ without loss of generality and used $m_{\rm A}\Delta\boldsymbol{v}_{\rm A} + m_{\rm B}\Delta\boldsymbol{v}_{\rm B} = 0$. Summation $(\sum_{\rm col})$ is done for all collisions with $r_{\rm A} < r < r_{\rm B}$ during a unit time.

We also average $F_{\rm col}$ over the region $[r - \frac{1}{2}r_0, r + \frac{1}{2}r_0]$ to be consistent with $\overline{F_{\rm local}}$ and for the summation to have enough number of collisions. Introducing $\Delta l = -m_{\rm A} r_{\rm A} \Delta v_{\theta{\rm A}}$,

$$\overline{F_{\rm col}} = \sum_{\rm col} \frac{S}{r_0} \Delta l, \tag{26}$$

where summation is taken over all collisions in the region $[r - \frac{1}{2}r_0, r + \frac{1}{2}r_0]$, during a unit time, and S is radial distance by which angular momentum Δl is transferred, i.e., $r_{\rm B} - r_{\rm A}$. To avoid duplicate counting, $S = r_{\rm B} - (r - \frac{1}{2}r_0)$ or $S = (r + \frac{1}{2}r_0) - r_{\rm A}$ for the collisions which straddle the boundary $r - \frac{1}{2}r_0$ or $r + \frac{1}{2}r_0$.

2.3.3. Gravitational angular momentum transfer

Substituting equation (19) into equation (12), we obtain $F_{\rm grav}$ in particle image as

$$\begin{aligned} F_{\rm grav}(r) &= -\int_{r_{\rm min}}^{r} dr' \int_0^{2\pi} r'd\theta \int_{-\infty}^{\infty} dz \int d\boldsymbol{v} r' v_\theta \left(\frac{\partial g}{\partial t}\right)_g \\ &= -\sum_{r_i<r} m_i r_i \left(\frac{\partial}{\partial t} v_{\theta,i}\right)_g = -\sum_{r_i<r} T_i^{\rm grav}, \end{aligned} \quad (27)$$

where $T_i^{\rm grav}$ is the torque exerted on particle i by mutual gravity. Apparently, $-F_{\rm grav}$ is total torque exerted on particles inside the radius r. Since the same amount of torque is exerted on particles outside r as recoils, $F_{\rm grav}$ is the angular momentum flux through a cylinder of radius r. We also average $F_{\rm grav}$ over the range $[r - \frac{1}{2}r_0, r + \frac{1}{2}r_0]$,

$$\overline{F_{\rm grav}}(r) = -\sum T_i^{\rm grav} - \sum \frac{r_i - (r - \frac{1}{2}r_0)}{r_0} T_i^{\rm grav}, \quad (28)$$

where the first summation is taken over all particles with $r_i < r - \frac{1}{2}r_0$, and the second summation is taken over all particles in the range $[r - \frac{1}{2}r_0, r + \frac{1}{2}r_0]$.

2.4. Properties of Angular Momentum Transfer

In a spatially uniform particulate disk with high optical depth, $F_{\rm col}$ is important (Araki & Tremaine 1986), since the sum of particle radii is larger than a mean free path of particles, so that more angular momentum is directly transfered by collisions, than by the excursions of the particles. In the region near planet's surface, where a tidal effect of the central planet is large, distribution of particles tends to be spatially uniform and $F_{\rm col}$ dominates angular momentum transfer (Takeda & Ida 2001; Daisaka, Tanaka & Ida 2002). However, in most region of the disk, spiral structure develops if the optical depth is high enough (Salo 1995; Daisaka & Ida 1999), and the disk is not spatially uniform (see snapshots of our simulations in Figs. 4). In this case, angular momentum transfer rate is regulated by surface density of the disk through the spiral structure (Takeda & Ida 2001; Daisaka, Tanaka & Ida 2002), and $F_{\rm trans}$ and $F_{\rm grav}$ dominate the angular momentum transfer.

2.4.1. Angular momentum transfer rate when the spiral structure develops

Under WKB approximation, spiral structure transfers angular momentum outward (Lynden-Bell & Kalnajs 1972) as

$$F_{\rm grav} = \frac{\pi}{2} G r^2 \lambda H^2 \sin i \cos^2 i, \tag{29}$$

where i, H, and λ are a pitch angle, a density amplitude, and a wave length of the spiral (Larson 1984). In the linear theory, the wave length is (e.g. Binney & Tremaine 1987)

$$\lambda = \frac{2\pi^2 G\Sigma}{\Omega^2}. \tag{30}$$

With numerical results $H \sim \Sigma$ and $\sin i \cos^2 i \sim O(1)$,

$$F_{\rm grav} \sim \frac{\pi^3 G^2}{\Omega^2} r^2 \Sigma^3. \tag{31}$$

When spiral structure develops, each spiral arm moves as if a super particle with collision frequency $\sim \Omega$, and Toomre's Q value $(= v_{\rm r}\Omega/\pi G\Sigma)$ (Toomre 1964) is $\sim O(1)$ (Salo 1995; Daisaka & Ida 1999), where $v_{\rm r}$ is radial random velocity of particles. Thus,

$$v_{\rm r} \sim \frac{\pi G \Sigma}{\Omega}. \tag{32}$$

Analogously to molecular viscosity, viscosity due to random motion is of the order of $v_{\rm r}^2 \Omega^{-1}$. Thus, from eqs. (18) and (32),

$$F_{\rm trans} \sim \frac{\pi^3 G^2}{\Omega^2} r^2 \Sigma^3. \tag{33}$$

Note that eqs. (31) and (33) have the same form.

In the case that spiral structure develops, $F_{\rm grav}$ and $F_{\rm trans}$ dominate over $F_{\rm col}$. Thus, angular momentum transfer rate has a form (eq. (18))

$$3\pi\Sigma r^2 \Omega \nu = C \frac{\pi^3 G^2}{\Omega^2} r^2 \Sigma^3, \tag{34}$$

where C is a numerical factor. In terms of viscosity,

$$\nu = \frac{C}{3} \frac{\pi^2 G^2}{\Omega^3} \Sigma^2. \tag{35}$$

The form of eq. (35) is consistent with a form of turbulent viscosity predicted by a dimensional analysis in Lin & Pringle (1987) or Ward & Cameron (1978). In general, C depends on r and about 2-10 within the region $r = [0.6 - 1.0]R_{\rm R}$, (Daisaka, Tanaka & Ida 2002; Takeda & Ida 2001).

2.4.2. Validity of the equation (34)

Expression eq. (34) assumes that the spiral structure regulates angular momentum transfer. This assumption is valid if the disk consists of many particles with number enough to represent the spiral structure. The validity of the expression eq. (34) depends on optical depth τ. A surface density Σ and an optical depth τ are given as

$$\Sigma = \frac{4}{3}\pi\rho r_{\rm p}^3 n, \tag{36}$$

$$\tau = \pi r_{\rm p}^2 n = \frac{3\Sigma}{4\rho r_{\rm p}}, \tag{37}$$

where n is a surface number density. The number of particles in a scale of structure is $n\lambda^2$. From eq. (30), (36), and (37),

$$n\lambda^2 = \frac{64\pi^3\rho^2 r^6}{9M_{\rm c}^2}\tau^3. \tag{38}$$

The number $n\lambda^2$ must be greater than some numerical factor, which is greater than 1 at least. We denote this factor by f_τ. Thus, the condition that eq. (34) is valid is

$$\tau > \tau_{\rm min} = f_\tau^{1/3}\frac{1}{4\pi}\left(\frac{3M_{\rm c}}{\rho r^3}\right)^{2/3}, \tag{39}$$

where f_τ is a numerical factor of order $\gtrsim 1$.

In Figs 2, we show the dependency of numerical factor C on optical depth τ at $r = 0.7R_{\rm R}$. The figures are from Takeda & Ida (2001). $C_{\rm g}$ and $C_{\rm t}$ represent the contributions to C of $F_{\rm grav}$ and $F_{\rm trans}$ respectively. In this region, $\tau_{\rm min}$ given by eq. (39) is $0.16 f_\tau^{1/3}$. Numerical results that C takes a constant value of order of 1 with large $\tau \gtrsim 0.2$ is consistent with above arguments.

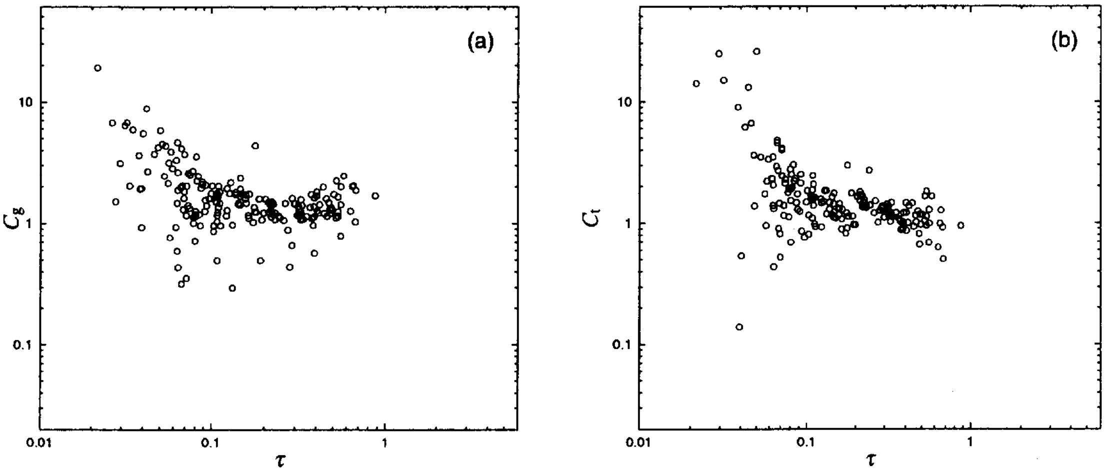

Fig. 2.— Relations between numerical factors $C_{\rm g}$ and $C_{\rm t}$ against optical depth τ (Figures from Takeda & Ida (2001)).

With a given disk mass, optical depth is an increasing function of particle number N. A disk consists of large number of particles has larger τ, while a disk consists of small number of particles has smaller τ. Since C is constant in the region $\tau > \tau_{\rm min}$, viscous evolution of two disks with different number of particles are similar, if eq. (39) is satisfied in both disks. Thus, we have no need to simulate the evolution of a disk with countless number of particles. Instead, we only have to simulate a disk with minimum number of particles which satisfies eq. (39). A minimum number of particles is given as follows. The averaged optical depth within a disk with an outer edge at $R_{\rm R}$ is

$$\tau = \frac{N\pi r_{\rm p}^2}{\pi(R_{\rm R}^2 - R_{\rm c}^2)} = \frac{1}{1-0.34^2}\left(\frac{3M_{\rm disk}}{4\pi\rho R_{\rm R}^3}\right)^{2/3} N^{1/3}. \tag{40}$$

Thus,

$$N \gtrsim 1.5\times 10^6 \tau_{\rm min}^3 \left(\frac{M_{\rm disk}}{0.01M_{\rm c}}\right)^{-2} \tag{41}$$

is a minimum number of particles needed to express the disk. If we take $\tau_{\rm min} = 0.25$, particle number must be greater than 20,000 for the disk with $M_{\rm disk} = 0.01M_{\rm c}$. However, more particles are in need initially, since particle number decreases with time. In our simulations, above condition is satisfied in the cases that a secondary satellite is formed until the formation time. However, this condition is not satisfied in the very last stage of some runs.

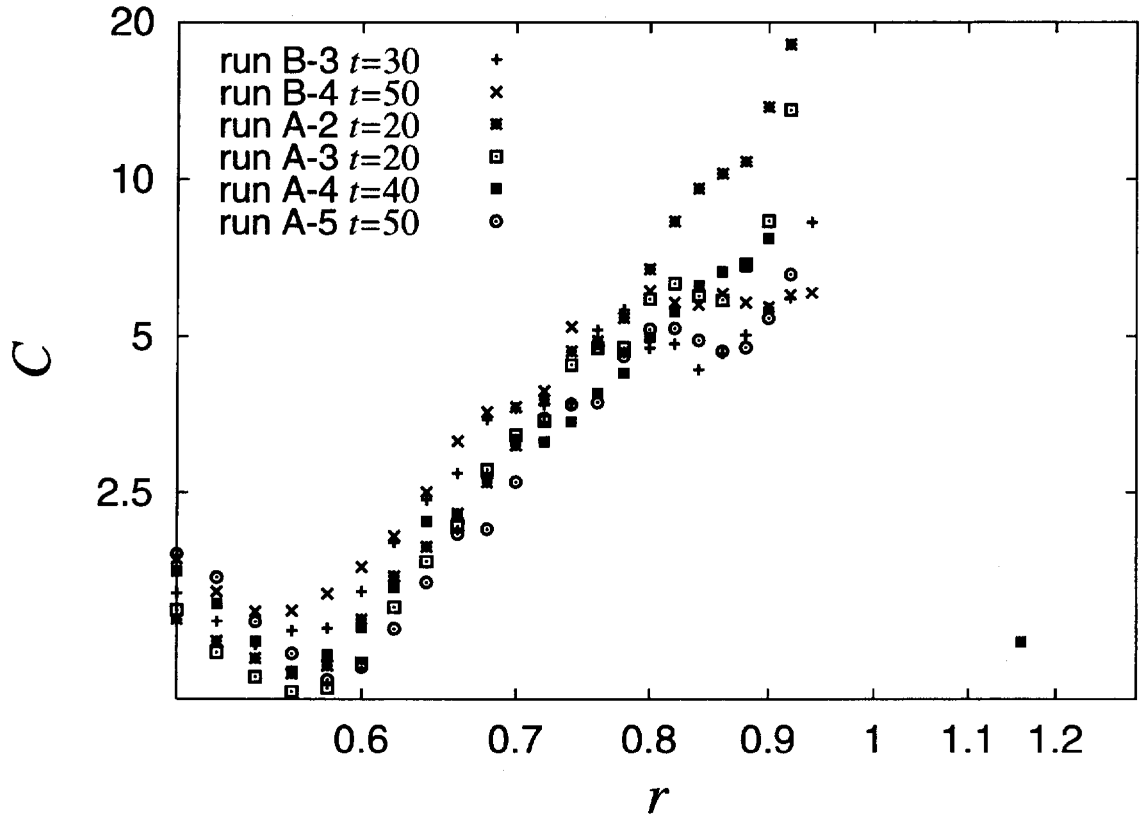

Fig. 3.— Distribution of the factor of angular momentum transfer C. Sampling times are chosen to be just before $t_{\rm stop}$ for each run.

2.4.3. Comparison with numerical result

We compare the factor C in our numerical simulations with the previous results. We show the distribution of C in our simulations in Fig. 3. The points in the figures show C as a function of r. These points are taken from the runs A-2, A-3, A-4, A-5, B-3 and B-4. The sampling times are the time at which the growth of a primary satellite stops (see below), and these points are taken only if optical depth > 0.15. The factor C is within the range [2-10], and C increases with r. This is consistent with the result of local N-body simulations (Daisaka, Tanaka & Ida 2002).

2.5. Diffusion Time Scale and Satellite Accretion

When disk materials diffuse beyond the Roche limit, particles begin to coagulate to form satellite seeds. The time scale of viscous evolution is given as $\sim \Delta r^2/\nu$, where Δr is a radial scale length of a disk. From eq. (35), the time scale of the evolution of a disk within Roche limit is given as (Kokubo, Ida & Makino 2000; Takeda & Ida 2001)

$$t_{\rm ev} \simeq \frac{500}{C}\left(\frac{\Sigma}{0.01 M_{\rm c} R_{\rm R}^{-2}}\right)^{-2}\left(\frac{\Delta r}{R_{\rm R}}\right)^{2}\left(\frac{r}{R_{\rm R}}\right)^{-9/2} T_{\rm K}. \tag{42}$$

In the case of a protolunar disk, $t_{\rm ev}$ is of order of $10 - 100 T_{\rm K}$.

Satellite seeds grow with particles which diffuse beyond the Roche limit. In most cases, one of the satellite seeds grows to a single large satellite. In the simulations of Kokubo, Ida & Makino (2000), a second massive moonlet with mass more than 20% of the most massive satellite is formed in only 6 of 60 runs. These second massive satellites survive from the collision to the largest satellite by being in a horse shoe orbit of the largest satellite. Growth of the satellite continues until the satellite becomes massive enough to form a gap between the disk and itself, and supplies of mass from the disk stops. We describe gap formation process in section 4.

3. NUMERICAL METHODS AND MODEL

3.1. Numerical Methods

Here, we briefly describe the simulation method used in the present study. We simulated the evolution of a debris disk by N-body method. We used 100,000 particles to represent the disk. We followed the orbital evolution of all particles by integrating the equations of motion:

$$\frac{d\boldsymbol{v}_i}{dt} = -GM_{\rm c}\frac{\boldsymbol{x}_i}{|\boldsymbol{x}_i|^3} - \sum_{j\neq i}^{N} Gm_j\frac{\boldsymbol{x}_i - \boldsymbol{x}_j}{|\boldsymbol{x}_i - \boldsymbol{x}_j|^3}. \tag{43}$$

The method of simulation and analysis of angular momentum transfer are nearly the same to the previous paper Takeda & Ida (2001) except for integrator. In the previous paper, we have used GRAPE-4 system (Makino, Taiji, Ebisuzaki, & Sugimoto 1997) which is a high-speed single-purpose computer for calculation of gravitational interaction between multiple particles. Since this system returns accelerations $d^2\boldsymbol{x}_i/dt^2$ and jolts $d^3\boldsymbol{x}_i/dt^3$, we had adopted 4th ordered Hermite scheme (Makino & Aarseth (1992)). In this paper, we use GRAPE-5 system (Kawai, Fukushige, Makino & Taiji 2000) which does not return jolts, so that we use 2nd ordered scheme with a smaller interval between each time step.

We include the collisions of particles in the calculation. When we detect $|\boldsymbol{x}_i - \boldsymbol{x}_j|$ becomes smaller than sum of particle radii $(r_i + r_j)$, we change velocities of particles according to restitution coefficient. We assume that all particles are perfectly smooth spheres, with tangential restitution coefficient $\epsilon_t = 1$ (free slip condition), neglecting the exchange between orbital angular momentum and spin angular momentum (Kokubo, Ida & Makino 2000). We use constant value 0.1 for normal restitution coefficient ϵ_n. The specific choice of ϵ_n does not effect angular momentum transfer in a disk much, as long as $\epsilon_n \lesssim 0.6$ (Takeda & Ida 2001). For detailed adjustment of collision and rebounding to avoid numerical difficulty, we follow Richardson (1994).

Outside the Roche limit, particles coagulate and form aggregates, which we call satellite seeds. To represent them, we adopt rubble pile model without any artificial accretion between particles. This is because satellite seeds often migrate or be scattered into the Roche limit by mutual interactions. Using rubble pile model, we can treat the destruction of these seeds when they reenter Roche limit. However, rubble pile model is time consuming, so that we change an aggregate to a single large particle if the aggregate is well outside Roche limit and the peril of reentering to the Roche limit no longer exists.

In this work, we assume that the central planet is spherical, neglecting deformation. We concentrate on a particulate disk, and neglect the gas component of the disk. We also neglect disruption, melting or vaporization of particles by collisions. Note that they would be important in a massive disk such as a protolunar disk.

In our simulations, we use M_c, R_R and $T_K/2\pi$ as units of mass, distance and time respectively, following Ida, Canup & Stewart (1997). In this case, the gravitational constant G becomes 1. For our adopted disk material density ρ (3.3 gcm^{-3}), Kepler time at $r = R_R$ is about 7 hr (which we denote as T_K).

3.2. Parameters, Models and Initial Conditions

In this work, we perform two sets of simulations. In one set of runs, particles are initially distributed from $0.4R_R$ to $1R_R$ with surface density $\Sigma(r) \propto r^{-3}$. For simplicity, particle size are all equal. With this surface density distribution, $l^0_{\rm disk} = 0.78\sqrt{GM_cR_R}$. We call this set of runs as set A. We performed 7 runs of set A with initial disk mass $M^0_{\rm disk}$ from 0.0098 to 0.0463 M_c. In another set, which we call set B, we initially put a satellite seed with mass M^0_s about 1.2 R_R. In this set, we allow artificial accretions between the satellite and particles. In this way, distinction between satellite and disk particles is easier, and we can use larger number of particles than set A to represent the disk, while artificial accretion reduces particle number quickly and allows faster calculation. We have confirmed that the existence an artificial satellite seed does not change the results as long as M^0_s is initially not large enough to form a gap, and the artificial satellite seed does not enter the Roche limit in its course of the growth. In set B, we performed three series of simulations with different initial specific angular momentum $l^0_{\rm disk} = 0.73, 0.78$, and 0.83 respectively. The initial surface density of each series is $\Sigma(r) \propto r^{\alpha}$, with $\alpha = -2, -3$, and -4. We performed 5 runs with $l^0_{\rm disk} = 0.78$, which has the same $l^0_{\rm disk}$ with the runs of set A, and 4 and 3 runs with $l^0_{\rm disk} = 0.73$ and 0.83 respectively. We describe initial conditions of each run in Table 1.

Table 1. Parameters of initial disks

RUN	$M^0_{\rm disk}$	$M^0_{\rm s}$	$M^{-\infty}_{\rm disk}$	$l^0_{\rm disk}$
RUN A-1	0.046	-	-	0.78
RUN A-2	0.037	-	-	0.78
RUN A-3	0.027	-	-	0.78
RUN A-4	0.022	-	-	0.78
RUN A-5	0.017	-	-	0.78
RUN A-6	0.012	-	-	0.78
RUN A-7	0.0098	-	-	0.78
RUN B-1	0.0390	0.0025	0.046	0.78
RUN B-2	0.0293	0.0025	0.036	0.78
RUN B-3	0.0195	0.0025	0.027	0.78
RUN B-4	0.0146	0.0025	0.022	0.78
RUN B-5	0.0145	0.0010	0.017	0.78
RUN B-6	0.0677	0.0020	0.075	0.73
RUN B-7	0.0484	0.0030	0.060	0.73
RUN B-8	0.0386	0.0025	0.048	0.73
RUN B-9	0.0290	0.0020	0.036	0.73
RUN B-10	0.0295	0.0030	0.036	0.83
RUN B-11	0.0196	0.0020	0.024	0.83
RUN B-12	0.0147	0.0010	0.017	0.83

4. RELATION BETWEEN SATELLITE MASS AND DISK MASS

As described in section 1, whether a single satellite system or multiple satellite system is formed depends on the mass of a satellite and the mass of the remaining disk. If the mass of a satellite were small compared with the remaining disk, the satellite migrate outward and a secondary satellite would be formed from the disk near the Roche limit. In this section, we show numerical results, and describe the relation between satellite mass and initial disk mass. In section 5, we determine the conditions to secondary satellite formation.

4.1. Overview of Disk Evolution and Satellite Accretion

In this subsection, we show typical evolution of disks for both cases that a single satellite is formed and that two satellites are formed.

4.1.1. Formation of a primary satellite

At first, we show the formation process of a primary satellite. In Figs. 4, we show the evolution of run A-3 (run without an artificial satellite seed). The circle at the center of each panel represents a central planet with $R_c = 0.34R_R$, while the largest circle represents $r = 1R_R$. Spiral structure develops in the disk immediately. At $t = 10$ (panel (a)), several satellite seeds are formed outside the Roche limit. By the time $t = 30$ (panel (b)), one large satellite is formed. After a few Kepler times, the satellite begins to migrate outward and the growth rate of the satellite decreases (see below). At $t = 80$ (panel (c)), a clear gap is formed between the disk and the satellite. The growth of the satellite is already stopped and the satellite is migrating outward. We show a snapshot at $t = 30$ in $r - z$ coordinates in panel (d). Large three circles indicate $r = R_c, 0.5R_R$, and $1R_R$ respectively. The satellite exists at $r = 1.2R_R$. The scale height of the disk is smaller than the satellite size, so that the two-dimensional treatment of disk-satellite interaction is reasonable.

It is known that a satellite and a disk repel each other by mutual interaction (Goldreich & Tremaine 1979). After the primary satellite is formed, it migrates outward, while disk particles fall to the central planet and disk mass diminishes. The outcome of the disk evolution depends on the mass of a primary satellite and the disk.

4.1.2. The case that only one satellite is formed

We show the evolution of disks after the formation of a primary satellite. In this subsection we show the case that another satellite is not formed. In Figs. 5, we show the evolution of run B-2 (a run with an artificial satellite seed). Panel (a) shows the snapshot of an initial disk and the satellite seed ($t = 0T_{\rm K}$). At $t = 20T_{\rm K}$, a gap is formed and the growth of the satellite stops, and the satellite begins to migrate (panel (b)). Initially, the edge of the gap moves outward as the satellite migrate outward (panel (c) at $t = 300T_{\rm K}$). However the disk edge never crosses the Roche limit well (panel (d) at $t = 800T_{\rm K}$). At this time, the disk has only 35% of the satellite mass, and the entire disk is within the Roche limit. A secondary satellite of considerable mass would no longer be formed from the disk. We stopped the simulation of this run at $t = 800T_{\rm K}$. The final outcome is a single satellite and some remnant disk materials, which does not have enough mass to spawn a secondary satellite with considerable mass. The disk would be cleared away by the satellite eventually (Ida, Canup & Stewart 1997; Kokubo, Ida & Makino 2000).

4.1.3. The case that a secondary satellite is formed

In this subsection, we show the case that a secondary satellite is formed. Figures 6 show the disk evolution of run B-4. The disk is less massive one than that of run B-2, and we initially set a satellite seed.

Panel (a) shows a snapshot at $t = 50T_{\rm K}$. By this time, a gap is formed, and growth of the satellite stops. Panel (b) shows a snapshot at $t = 200T_{\rm K}$. Considerable mass is already outside the Roche limit, and temporal aggregates are formed. However, the disk edge is near 1:2 resonance of the primary satellite, and these aggregates have relatively

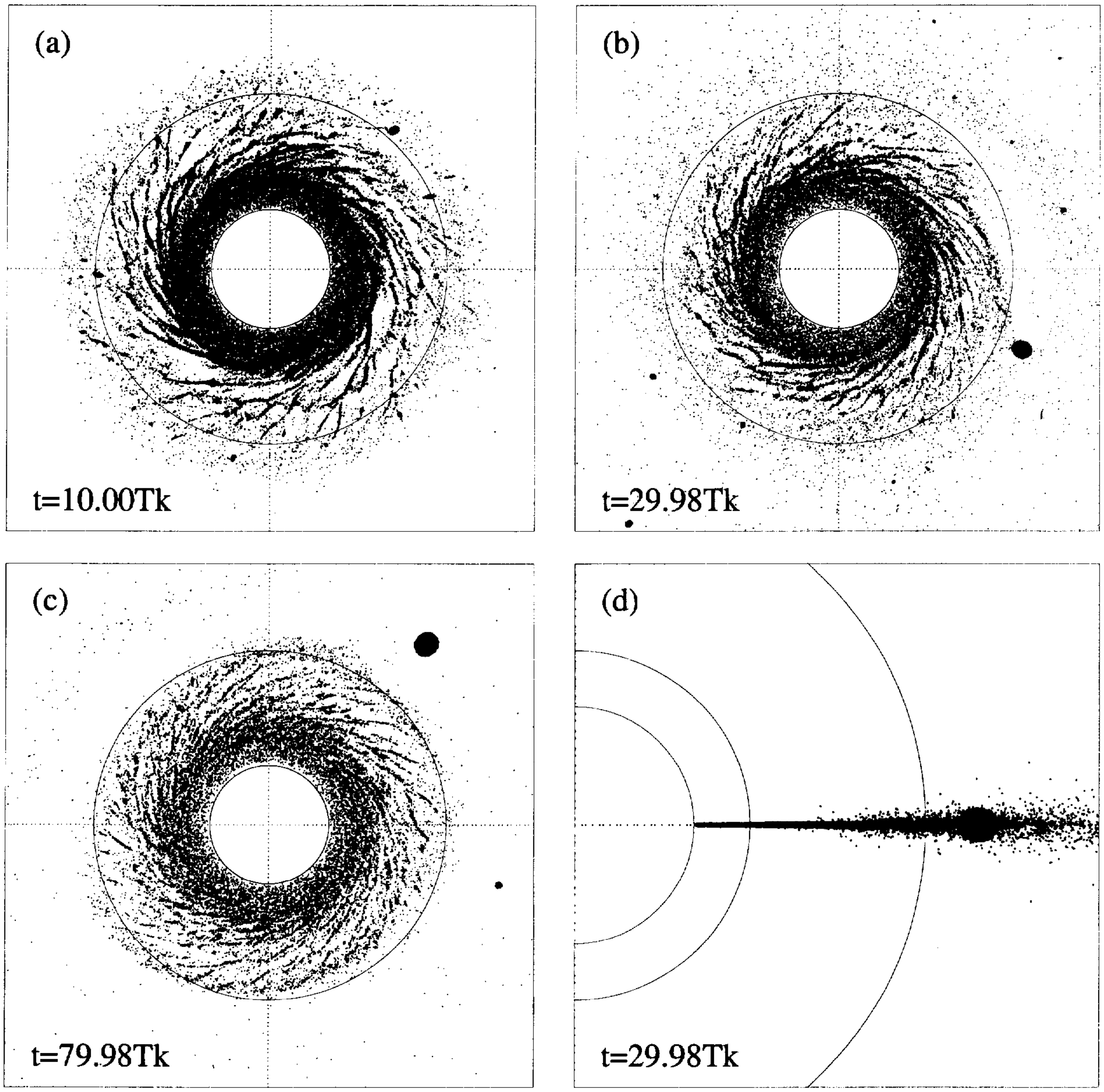

Fig. 4.— Snapshots of (a) run B-3 at $t = 10$, (b) $t = 30$ and (c) $t = 80$. We draw three circles at center in each panel with $r = R_{\rm P}$, $r = 0.5R_{\rm R}$ and $r = R_{\rm R}$ as a guide. Panel (d) is snapshot in r-z plane. the meaning of three circles are the same.

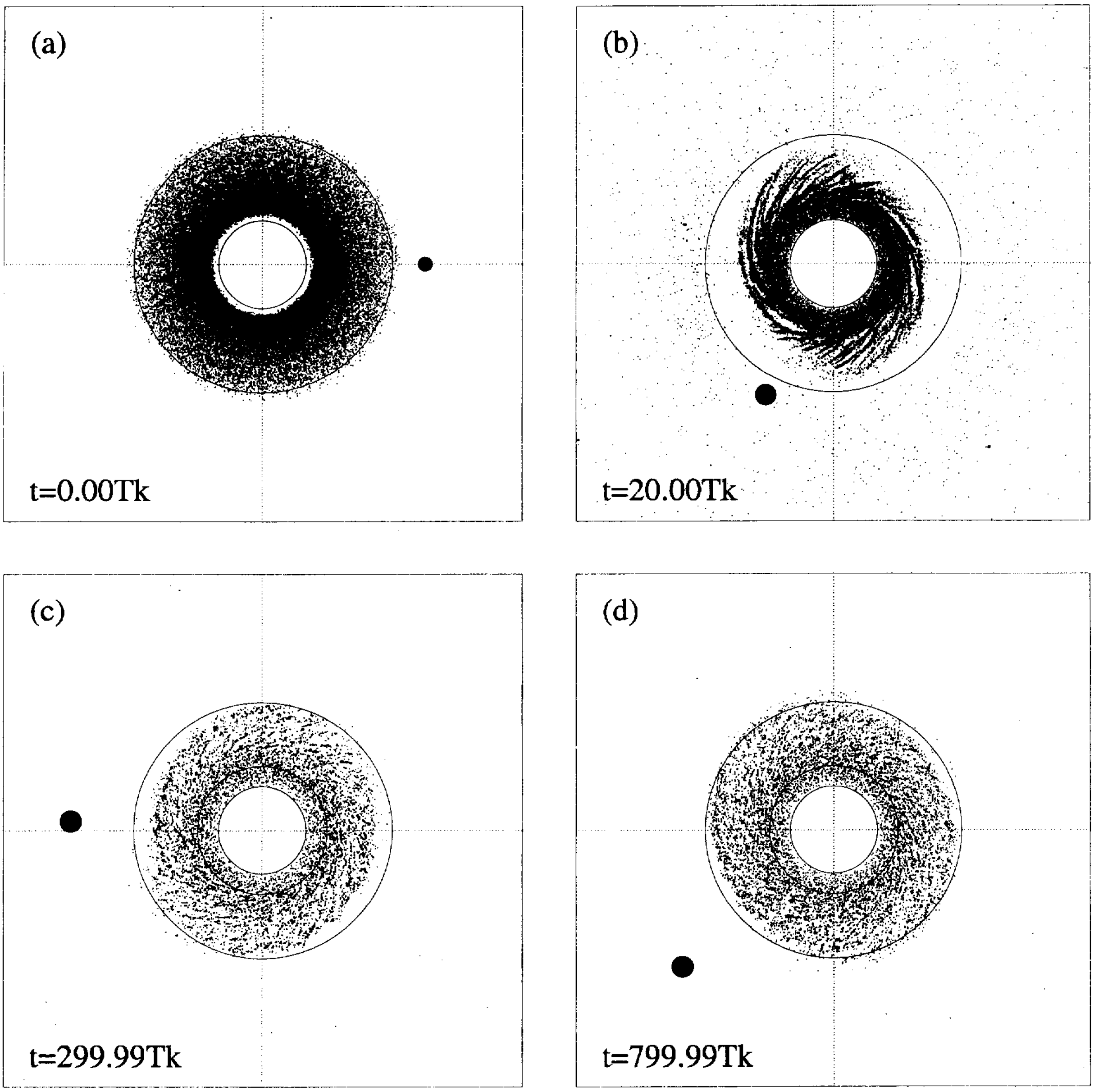

Fig. 5.— Snapshots of run B-4 (run with an artificial satellite seed). panel (a)-(d) are snapshots at $t = 0, 20, 300, 800 T_{\rm K}$ respectively. Three circles in each panel indicates $r = R_{\rm c}$, $r = 0.5 R_{\rm R}$ and $r = R_{\rm R}$. A relatively large particle just outside Roche limit in panel (a) is a satellite seed of the primary satellite.

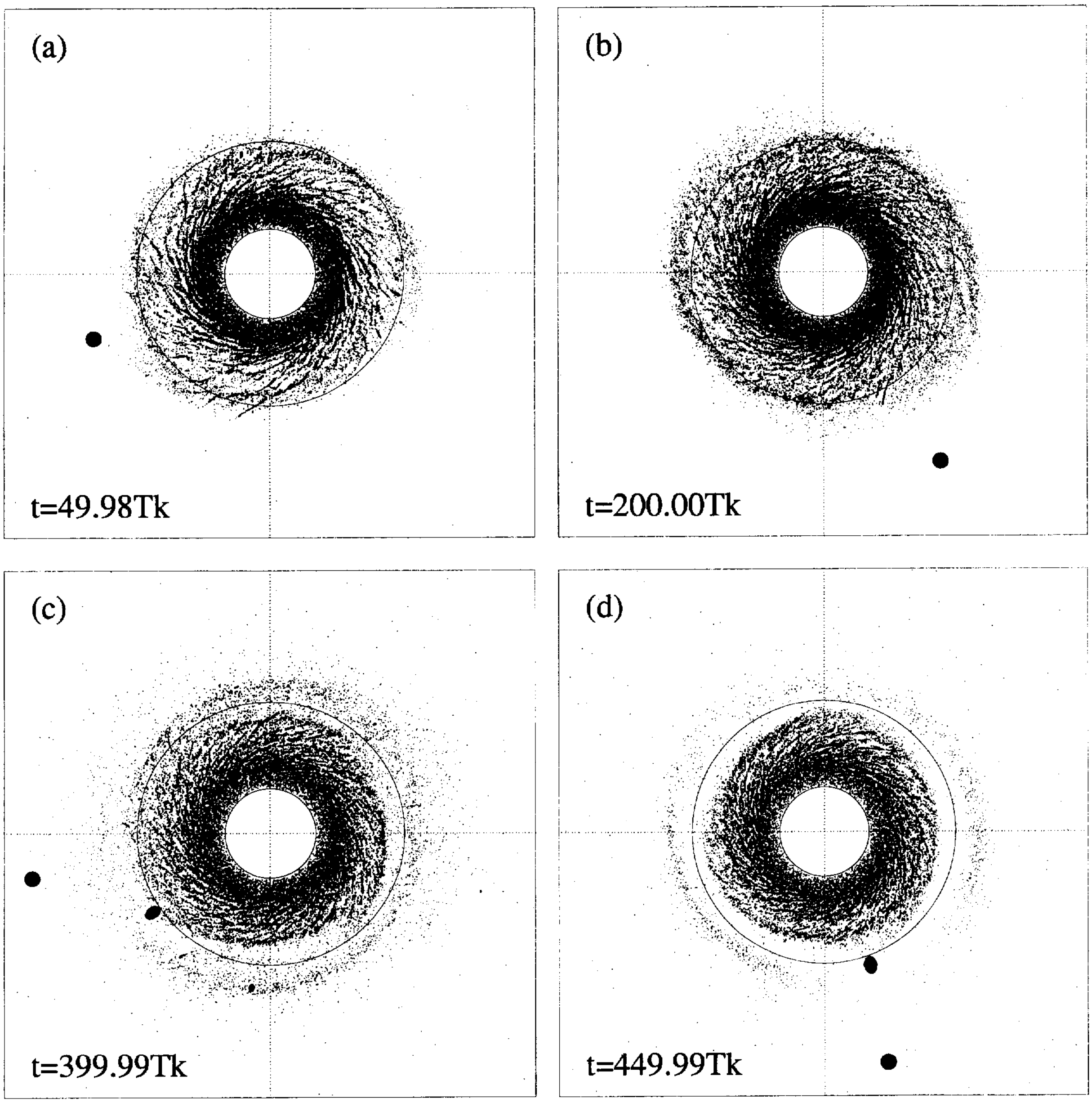

Fig. 6.— Snapshots of run B-4 (run with an artificial satellite seed). Panel (a)-(f) are snapshots at $t = 50, 200, 400, 450 T_{\rm K}$, respectively. Three circles in each panel indicates $r = R_{\rm c}$, $r = 0.5R_{\rm R}$ and $r = R_{\rm R}$ as before.

large eccentricities and enter the Roche limit at pericenter, and are destroyed. Thus, a secondary satellite is not formed yet. Panel (c) shows the snapshot at $t = 400T_K$. The Primary satellite migrates further away and formation of a secondary satellite begins at the disk edge. At $t = 450T_K$ (panel (d)), the formation of the secondary satellite is almost complete, and a two-satellite system is formed.

4.1.4. Mass of a primary satellite

Whether multiple satellite system is formed or not depends on the mass of the primary satellite and the disk mass. In Fig. 7, we show the relation between the initial disk mass $M^0_{\rm disk}$ and final satellite mass of runs of set A (runs without artificial satellite seed). Filled circles are the mass of the most massive aggregate at the end of each simulation. Mass of the satellite decreases with decreasing disk mass. Satellite mass is roughly proportional to square of the disk mass [$M_{\rm s} \propto (M^0_{\rm disk})^2$]. As shown below, the mass ratio between the satellite $M_{\rm s}(t_{\rm stop})/M_{\rm disk}(t_{\rm stop})$ also decreases as $M^0_{\rm disk}$ decreases. Here we denoted a time at which growth of a satellite stops by $t_{\rm stop}$. The satellite and the remaining disk repel each other. If $M_{\rm s}(t_{\rm stop})/M_{\rm disk}(t_{\rm stop})$ were large, disk particles would fall to the central planet by disk-satellite interaction. If $M_{\rm s}(t_{\rm stop})/M_{\rm disk}(t_{\rm stop})$ were small, the satellite would be repelled outward instead. If the primary satellite migrates enough, the edge of the disk reaches the Roche limit again, and a secondary satellite would be formed near the Roche limit. This leads to two different outcomes of the evolution of a debris disk, depending on the disk mass:

(a) A massive disk forms a relatively massive satellite. In this case, disk mass falls to the central planet, while satellite is repelled by the disk outward only a little. The decrease of disk mass and its viscosity are faster than the satellite migration. Therefore, the disk mass does not reach the Roche limit, and all disk materials are lost to the central planet finally. Thus, if $M^0_{\rm disk}$ is larger than a certain critical mass $M^{\rm crit}_{\rm disk}$, the final outcome is a single satellite.

(b) From the less massive disk, a less massive satellite is formed. Thus, satellite

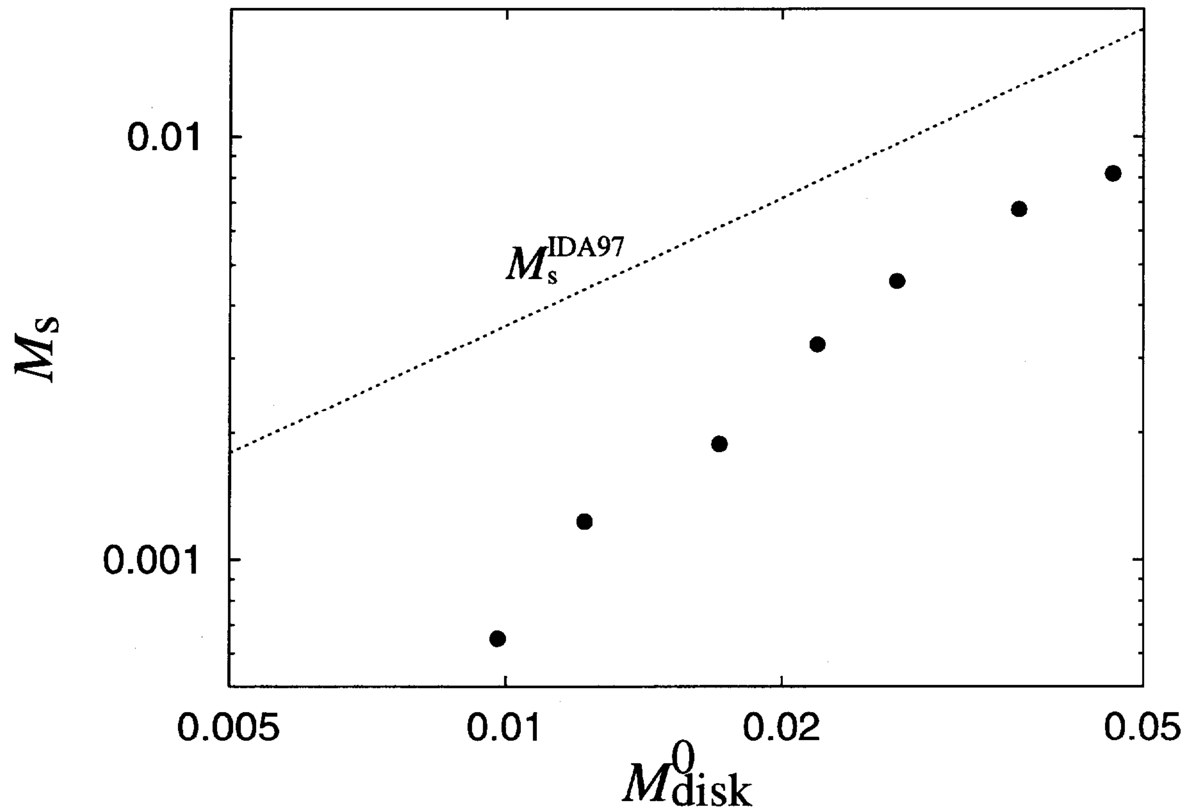

Fig. 7.— Relation between the initial disk mass and the final satellite mass.

migrates by large distance before disk mass decreases considerably. Thus, satellite migration is faster than decrease of disk mass and its viscosity, and the disk edge moves outward as the satellite migrates outward. When the disk edge migrates enough, secondary satellite formation occurs outside the Roche limit. Thus, if $M_{\rm disk}^0$ is smaller than $M_{\rm disk}^{\rm crit}$, the outcome is a multiple satellite system.

Our purpose is to quantitatively determine a critical mass $M_{\rm disk}^{\rm crit}$. Since the disk evolution is regulated by the relation of satellite mass and disk mass, we investigate the relation between them.

4.2. Conservation Laws of Mass and Angular Momentum

Satellite mass and disk mass are related by the conservation laws of mass and angular momentum (Ida, Canup & Stewart 1997):

$$M_{\rm disk}^0 = M_{\rm fall}(t) + M_{\rm disk}(t) + M_{\rm s}(t), \tag{44}$$

$$l_{\rm disk}^0 M_{\rm disk}^0 = l_{\rm fall}(t) M_{\rm fall}(t) + l_{\rm disk}(t) M_{\rm disk}(t) + l_{\rm s}(t) M_{\rm s}(t), \tag{45}$$

where $M_{\rm disk}, M_{\rm s}, l_{\rm disk}$, and $l_{\rm s}$ are mass and specific angular momentum of the disk and the satellite, and $M_{\rm fall}$ and $l_{\rm fall}$ are cumulative mass and average specific angular momentum of particles which fall to the central planet. Index 0 indicates $t = 0$. Here, we neglect the mass escapes from the system for simplicity. In general, $l_{\rm fall}$ is a constant about $r_{\rm c}^2 \Omega(r_{\rm c})$. We summarized the notations in Table 3.

In the case of lunar formation, a massive satellite is formed from a protolunar disk and all disk material falls to the Earth by disk-satellite interaction (Ida, Canup & Stewart 1997). In this case, $M_{\rm disk}^\infty = 0$. Then, from eqs. (44) and (45),

$$M_{\rm s}^{\rm IDA97} = M_{\rm s}^\infty = \left(\frac{l_{\rm disk}^0 - l_{\rm fall}}{l_{\rm s}^\infty - l_{\rm fall}} \right) M_{\rm disk}^0. \tag{46}$$

We denote final state ($t = \infty$) by index ∞. If the satellite is massive enough, the migration of the satellite is small, and final location of the satellite is near the Roche limit. In this case, $r_{\rm s}^\infty \sim 1.3 R_{\rm R}$, and since eccentricity of the satellite is small, $l_{\rm s}^\infty$ is about $(r_{\rm s}^\infty)^2 \Omega(r_{\rm s}^\infty)$ (Ida, Canup & Stewart 1997). Thus, final satellite mass is uniquely determined as a function of $M_{\rm disk}^0$ and $l_{\rm disk}^0$. We show $M_{\rm s}^{\rm IDA97}$ in Fig. 7 by dotted line. Note that $M_{\rm s}^{\rm IDA97}$ is proportional to $M_{\rm disk}^0$, while dependency of satellite mass on $M_{\rm disk}^0$ is stronger in numerical simulations. This difference comes from that assumptions $M_{\rm disk}^\infty = 0$ and $r_{\rm s}^\infty \sim 1.3 R_{\rm R}$ break down in the case of lower $M_{\rm disk}^0$.

Final location of a primary satellite depends on the satellite mass and disk mass at $t_{\rm stop}$, and whether a secondary satellite would be formed or not depends on the location of the primary satellite. Our first purpose is to derive $M_{\rm disk}(t_{\rm stop})$ and $l_{\rm disk}(t_{\rm stop})$ as functions of $M_{\rm s}(t_{\rm stop})$. With these relations, we can derive $M_{\rm s}(t_{\rm stop})$ and $M_{\rm disk}(t_{\rm stop})$ as functions of $M_{\rm disk}^0$ and $l_{\rm disk}^0$ using eqs. (44) and (45). Both $M_{\rm disk}(t_{\rm stop})$ and $l_{\rm disk}(t_{\rm stop})$ are determined by the gap formation condition between the satellite and the disk. We investigate the gap formation condition and give the relation between satellite mass and initial disk mass in the next subsection.

4.3. Gap Formation

A satellite grows with mass supply from the disk. However, as mentioned above, a satellite and a disk repel each other by mutual interaction (Goldreich & Tremaine 1979). Thus, as the satellite mass increases to a certain limit, it forms a gap between the disk and itself. Consequently, there exists an upper limit to the satellite mass which is formed from a circumplanetary disk which is initially confined within the Roche limit. The location of the disk edge is determined by the equilibrium between satellite-disk interaction and viscous spreading of the disk. Since the viscosity is determined by the disk surface density, the condition for gap formation is determined by the satellite mass and disk mass. In subsection 4.3.1 and 4.3.2 we describe the basic equations and disk-satellite interaction. We describe the surface density distribution and show detail of growth of satellites in numerical simulations in subsection 4.3.3, and describe gap formation conditions in subsection 4.3.4.

4.3.1. Basic equations of gap formation

In the following subsections, we derive the condition for gap formation. Viscous spreading of the disk is determined by viscous torque (eqs. (15) and (18)):

$$\dot{M}_{\mathrm{disk}} = -\frac{1}{\partial h/\partial r}\frac{\partial}{\partial r}\left(3\pi\Sigma r^2\Omega\nu\right). \tag{47}$$

The term $-(\partial/\partial r)3\pi\Sigma r^2\Omega\nu$ is angular momentum deposited by a viscous torque on a cylinder with the width of unit length at radius r. If a gap is formed, viscous torque works to fill the gap. With existence of external torque exerted on the disk, eq. (47) becomes

$$\dot{M}_{\mathrm{disk}} = -\frac{1}{\partial h/\partial r}\left\{\frac{\partial}{\partial r}\left(3\pi\Sigma r^2\Omega\nu\right) - T_{\mathrm{s}}\right\}, \tag{48}$$

where T_s is a torque density exerted on the disk. When a satellite grows massive enough, the external torque T_s from the satellite becomes important. By the interaction, angular momentum is transfered from the inner disk to the outer satellite (Goldreich & Tremaine 1980). Such an interaction acts to open a gap between a satellite and a disk, while the viscous torque acts to fill the gap. Thus, gap formation depends on balance between the viscous torque and the torque from the satellite.

We summarize here the properties of viscous torque again briefly. When a particle disk is optically thick enough, spiral pattern due to the gravitational instability develops. Then, angular momentum transfer rate is determined by the spiral pattern, which is regulated by surface density. Viscous angular momentum transfer rate is written as

$$3\pi\Sigma r^2\Omega\nu = C\frac{\pi^3G^2}{\Omega^2}r^2\Sigma^3. \tag{49}$$

The numerical factor C is increasing function of r. Within the region $r = [0.6 - 1.0]R_{\rm R}$, C takes value from 2-10.

4.3.2. Satellite-disk interaction

The derivation of disk-satellite interaction is given in several literatures (e.g., Goldreich & Tremaine 1982; Lin & Pringle 1993). We first consider the encounter of a disk particle and the satellite. We assume that $M_{\rm c} \gg M_{\rm s} \gg m_{\rm p}$, where $m_{\rm p}$ is mass of a particle, and a coplanar encounter, and that the orbit of the satellite is circular. Assuming that the semimajor axes of the satellite and the disk particle are close, relative motion can be described by Hill's equation (e.g., Nakazawa, Ida & Nakagawa (1989)). In this equation, time is scaled by the Keplerian angular velocity Ω_0 given by $\Omega_0^2 = GM_{\rm c}/a_0^3$, where a_0 is reference semimajor axis, which we define to be equal to the semimajor axis of satellite $r_{\rm s}$ here. Distance is scaled by the Hill radius $hr_{\rm s}$ where h is defined as

$$h = \left(\frac{M_{\rm s}}{3M_{\rm c}}\right)^{1/3}. \tag{50}$$

We adopt h including the factor $3^{-1/3}$. Note that some literatures adopt h without the factor $3^{-1/3}$.

We consider the orbit of a particle whose radial separation is b to the satellite. Since a disk particle is on an inner orbit, it overtakes the satellite. After an encounter, the radial separation becomes $b + \Delta b$. The change of radial separation Δb in the lowest order of b^{-1} is given as (Petit & Hénon 1984; Hasegawa & Nakazawa 1990)

$$\Delta b = \frac{128}{27}[2K_0(\frac{2}{3}) + K_1(\frac{2}{3})]^2 b^{-5}, \tag{51}$$

where K_0 and K_1 are modified Bessel functions. Though above formula is for the case that orbits of particle and satellite are initially circular, average of Δb is also given by eq. (51) when the longitudes of pericenter of particles are distributed uniformly (Petit & Hénon 1984; Hasegawa & Nakazawa 1990). In general, an encounter changes the longitude of pericenter at the next encounter. However, assuming that inter particle interaction smears out the effect of an encounter, we can derive the angular momentum transfer rate as successive distant encounters. This may be good approximation except near major resonances (Petit & Hénon 1984). Since $m_\mathrm{p} \ll M_\mathrm{s}$, the satellite moves outward $(m_\mathrm{p}/M_\mathrm{S})\Delta b$ during an encounter, while disk particle moves inward $-\Delta b$.

Since the interval of conjunction between the particle and the satellite is $T_\mathrm{sync} = (4\pi/3hb)$, the rate of the change of semimajor axis of particles is

$$\frac{dr}{dt} = \epsilon b^{-4} h, \tag{52}$$

where

$$\epsilon = \frac{32}{9\pi}[2K_0(\frac{2}{3}) + K_1(\frac{2}{3})]^2 = 7.2. \tag{53}$$

Note that above formulation assumes large b. Equation. (51) underestimates Δb when b is not so large (Ida 1990). We show Δb derived from numerical integration of 3-body problem in Fig 8. Solid line represents the Δb estimated by eq. (51). Filled circles are derived by numerical integration of 3-body problem. At large limit of b, eq. (52) and numerical result coincide. However, numerical result is larger than eq. (52), up to factor ~ 5 at $b \sim 2.5$. Since gap formation occurs in this region, we should multiply some factor to eq. (53). In our numerical simulations, surface density distribution is well explained when we adopt $\epsilon = 14.4$ (see below).

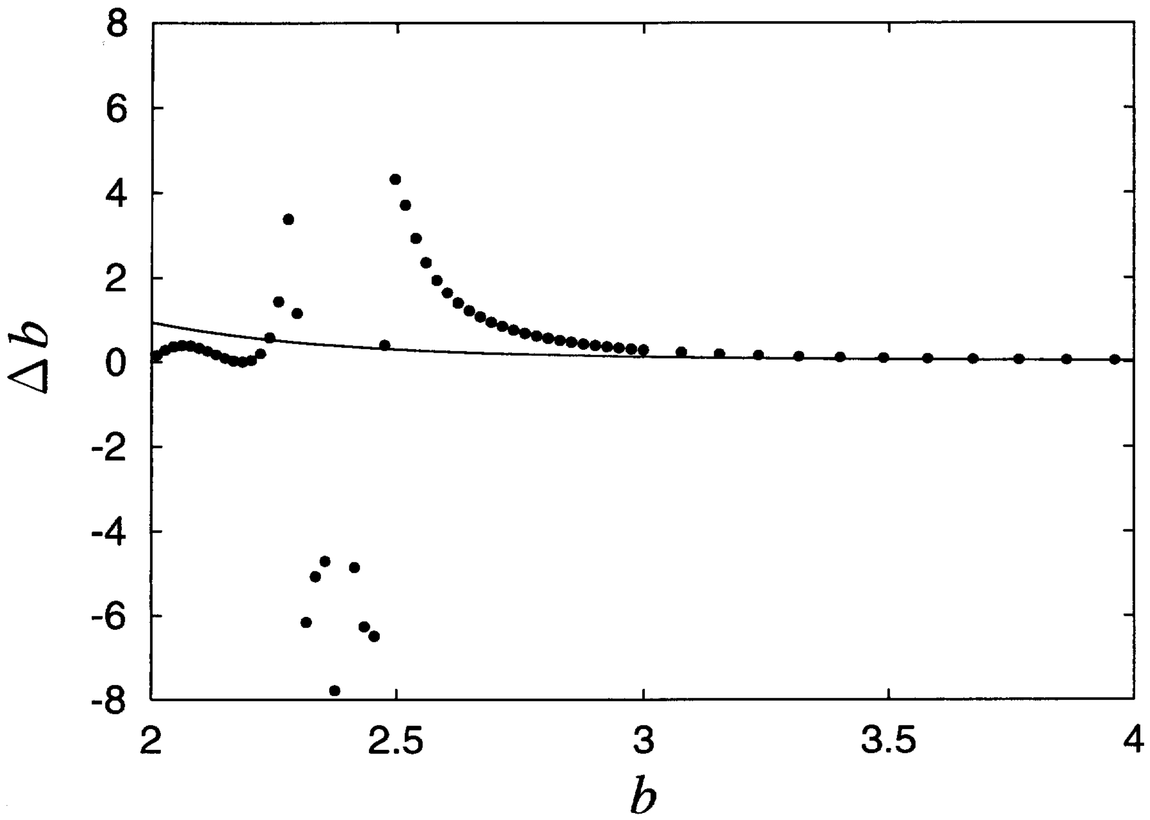

Fig. 8.— Comparison between analytical evaluation of Δb and numerical result. Solid line represent the estimated Δb (eq. (51)). Filled circles are derived by numerical integration of 3-body problem.

In the region $b > 2.5$, Δb has the same sign with b, so that disk-satellite interaction works as if it were a repulsive force. In the region $b < 2.5$, an encounter becomes a close encounter (Ida & Nakazawa 1989). A particle enters to the potential well of the satellite (Hill's sphere). In the region $2.3 < b < 2.5$, Δb has the opposite sign to b and the interaction works as an attractive force. Being near the Roche limit, physical radius of the satellite and the radius of the Hill's sphere are comparable, so that most of particles which enter the Hill's sphere collide to the satellite. In the case that $b < 1.8$, particle takes a horse shoe orbit and turns back. Accretion of particles to a satellite occurs in the region $1.8 < b < 2.5$. Particles in the region $[r_s - 1.8hr_s, r_s + 1.8hr_s]$ remain long in the numerical simulations (Fig. 6 panel (d)), being in horse shoe orbits. However, most of them diffuse from this region by particle-particle interaction eventually. Thus, we call the region $[r_s - 2.5hr_s, r_s + 2.5hr_s]$ the feeding zone of the satellite.

From the relation that the specific angular momentum of a particle $l = \sqrt{GM_c r}$, the change of specific angular momentum of a particle is $dl/dt = (l/2r)dr/dt$. Torque density is given by $2\pi\Sigma r(dl/dt)$. From eq. (52), torque density on the disk in the normal unit is

$$T_s = -\pi\epsilon r_s \Sigma \left(\frac{r_s - r}{hr_s}\right)^{-4} h^2 r_s^2 \Omega_0^2 = -\frac{\epsilon}{9}\left(\frac{\pi r_s^2 \Sigma}{M_c}\right)\left(\frac{GM_s^2}{r_s^2}\right)\left(\frac{r_s - r}{r_s}\right)^{-4}. \quad (54)$$

Here we replaced r by r_s unless they appear in the form $r - r_s$. Note that we can obtain a similar result to eq. (54) by averaging interactions of many resonances in the vicinity of the satellite (Goldreich & Tremaine 1980).

4.3.3. Surface density distribution

Since disk particles and a satellite repel each other, disk-satellite interaction works to clear out the disk near the satellite. On the other hand, viscous spreading of the disk works to fill the cleared region. As the satellite grows, the effect of disk satellite-interaction increases, and the satellite clears the disk particles and forms a gap.

In this subsection, we derive the surface density distribution when the satellite torque and the viscous torque are in equilibrium, using eq. (49) for viscous spreading and eq. (54) for satellite torque. In an equilibrium structure, Σ decreases and becomes 0 near the satellite. The location where Σ becomes 0 is the estimated location of the disk edge, which we denote by r_{eq}. The estimated width of the gap, $r_s - r_{eq}$ depends on the satellite mass and surface density of the disk far from the satellite. As explained in the previous section, when the gap width is smaller than $2.5hr_s$, eq. (54) breaks down. In this case, the particles near the disk edge closely encounter the satellite and collisions occur. Thus, the growth of the satellite continues if $r_s - r_{eq} < 2.5hr_s$. As the satellite grows and surface density decreases, the estimated width of the gap increases. When gap width reaches $2.5hr_s$, the growth of the satellite stops. At this time, the location of the disk edge in numerical simulation (r_{edge}), and estimated location r_{eq} are in agree as shown below. Finally, we derive a satellite mass at which $r_s - r_{eq}$ reaches $2.5hr_s$, which is an upper limit of the satellite mass.

Evolution of a surface density is regulated by viscosity of a disk and disk-satellite interaction. From the equation of continuity and eq.(48),

$$\frac{\partial \Sigma}{\partial t} = \frac{1}{2\pi r}\frac{\partial}{\partial r}\left[\frac{1}{\partial h/\partial r}\left\{\frac{\partial}{\partial r}(3\pi\Sigma r^2\Omega\nu) - T_s\right\}\right]. \tag{55}$$

If time scale of mass depletion of a disk and a migration time of a satellite are much longer than a relaxation time of surface density, a quasi-stationary state is achieved and we can approximate as $\partial\Sigma/\partial t = 0$. This assumption is generally valid since the outward migration of the satellite begins after a gap is well formed. Then

$$\frac{1}{\partial h/\partial r}\left\{\frac{\partial}{\partial r}(3\pi\Sigma r^2\Omega\nu) - T_s\right\} = \text{const.} \tag{56}$$

Since viscous torque and T_s are 0 outside the disk edge, the constant in eq.(56) is 0. Assuming that the torque from the satellite is important only in the vicinity of the satellite, we substitute eqs.(49) and (54) to eq.(56):

$$\frac{1}{\Sigma}\frac{\partial}{\partial r}(Cr^5\Sigma^3) + \frac{\epsilon}{9}\left(\frac{M_s^2}{\pi^2}\right)\left(\frac{r_s - r}{r_s}\right)^{-4} = 0. \tag{57}$$

The solution to eq.(57) is

$$(C^{1/3}\alpha^{5/3}\Sigma)^2 = -\frac{2}{27}\left(\frac{M_s}{\pi r_s^2}\right)^2 \int \epsilon C^{-1/3}\alpha^{-5/3}(1-\alpha)^{-4}d\alpha, \tag{58}$$

where $\alpha = r/r_s$.

Since the interaction is important only near the satellite, we simplify eq. (58) by replacing α in the integral by 1 except for the terms in the form $1-\alpha$. Also we approximate C as a constant. Introducing $F(\alpha)$ as

$$F(\alpha) = \int (1-\alpha)^{-4}d\alpha = \frac{1}{3}(1-\alpha)^{-3}, \tag{59}$$

eq. (58) is

$$\Sigma = \left(\frac{M_s}{\pi r_s^2}\right) C^{-1/3}\left(\frac{r}{r_s}\right)^{-5/3}\sqrt{A - \left(\frac{2\epsilon}{27}\right)C^{-1/3}F\left(\frac{r}{r_s}\right)}, \tag{60}$$

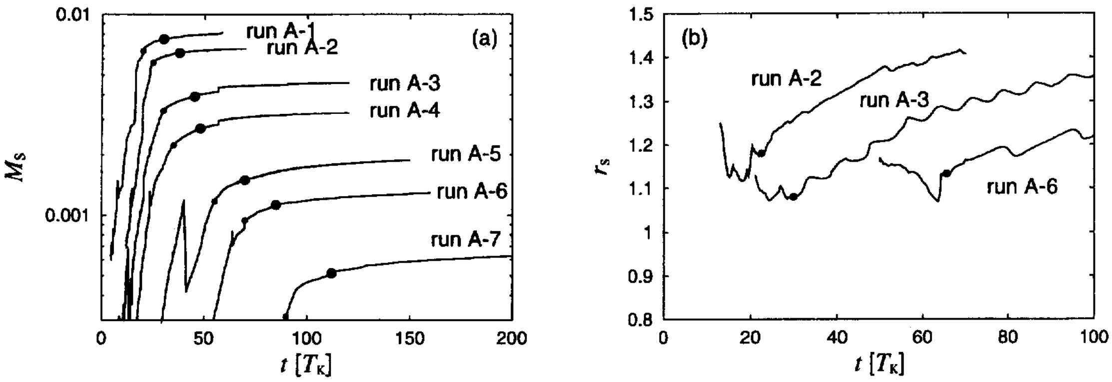

Fig. 9.— (a) Evolution of mass of a satellite for runs A (runs without an artificial satellite seed), and (b) evolution of semimajor axis of a satellite for run A-2, A-3 and A-6.

where A is a constant of integration. Defining Σ^* as

$$\Sigma^* = \left(\frac{M_s}{\pi r_{\rm s}^2}\right) C^{-1/3}\sqrt{A}, \tag{61}$$

eq. (56) is

$$\Sigma = \Sigma^* \left(\frac{r}{r_{\rm s}}\right)^{-5/3} \sqrt{1 - \left(\frac{2\epsilon}{27C}\right)\left(\frac{M_s}{\pi r_{\rm s}^2 \Sigma^*}\right)^2 F\left(\frac{r}{r_{\rm s}}\right)}. \tag{62}$$

In this subsection, we confirm the validity of surface density distribution given by eq. (62), comparing the surface densities in numerical simulations with eq. (62) at $t = t_{\rm stop}$. In the next subsection 4.3.4, we will derive a relation between Σ^* and satellite mass at $t = t_{\rm stop}$.

To compare eq. (62) to numerical result at $t = t_{\rm stop}$, we must determine $t_{\rm stop}$ in numerical simulations. We show evolution of masses and semimajor axes of satellites of runs of set A in Figs. 9. The satellite is defined as the most massive aggregate in each run.

Panel (a) shows the mass growth of satellites of numerical simulations from run A-1 to A-7. Initially, the satellite grows rapidly, then its growth rate decreases gradually and stops. In panel (b), we show the evolution of semimajor axis of run A-2, A-3 and A-6. Initially, a satellite seed does not migrate outward, or rather migrates inward. This is because the satellite grows with the disk particles whose orbital specific angular momentum is smaller than the satellite. Sometimes, it reenters the Roche limit and is disrupted (see the peak in mass growth of run A-5 in panel (a)). As the growth of satellite slows down, outward migration begins and growth of satellite stops eventually. Since the growth of satellite slows down gradually, it is not easy to determine $t_{\rm stop}$ clearly. Here we use the fact that outward migration begins just before gap formation. The filled circles in panel (b) represent the time at which the satellite begins to migrate outward (we denote this time as $t_{\rm mig}$). In panel (a), we put two points for each line. Small points represent $t_{\rm mig}$, and large points represent $t_{\rm grow}$ defined as follows. When the migration of satellite begins ($t = t_{\rm mig}$), the growth of the satellite is nearly finished, though the satellites continue its growth somewhat after $t_{\rm mig}$ in all runs. Thus, we defined $t_{\rm stop}$ in numerical simulations as $t_{\rm stop} - t_{\rm grow} = 1.5(t_{\rm mig} - t_{\rm grow})$, where $t_{\rm grow}$ is a time at which rapid growth of the satellite begins. We summarized the satellite mass and disk mass at stopping time in Table 2.

We show the surface density distribution at $t = t_{\rm stop}$ in Fig. 10, and we compare them with eq. (62). Panel (a) shows surface density of run A-2 at $t = 40$ and panel (b) shows surface density of run A-6 at $t = 90$. Solid lines are surface densities in numerical simulations, and dotted lines are surface density estimated by eq. (62). Here, we use surface density which is defined by the semimajor axes of particles rather than r, because the structure of the disk edge is clearer in this way. The constant of integration Σ^* is determined by fitting eq. (62) and surface density of numerical simulation at $r = 0.8R_{\rm R}$. This particular value is chosen so that it is apart from the disk edge and gradient of surface density is small, and in this region the spiral pattern well develops and the eq. (34) is valid. We also show the semimajor axis of the satellite of each run in the figure. In the estimation of eq. (62), we used $C = 5$ from the numerical result, and $\epsilon = 14.4$, which is two times larger than eq. (53). In both cases, estimations and surface densities in numerical simulations are in agreement in the region $r > 0.7R_{\rm R}$, and $r_{\rm eq} \sim r_{\rm edge}$. This indicates that gap formation is well described by the equilibrium between viscous torque and satellite torque. Numerical result shows somewhat steeper surface density distribution, which would come from r dependency of C.

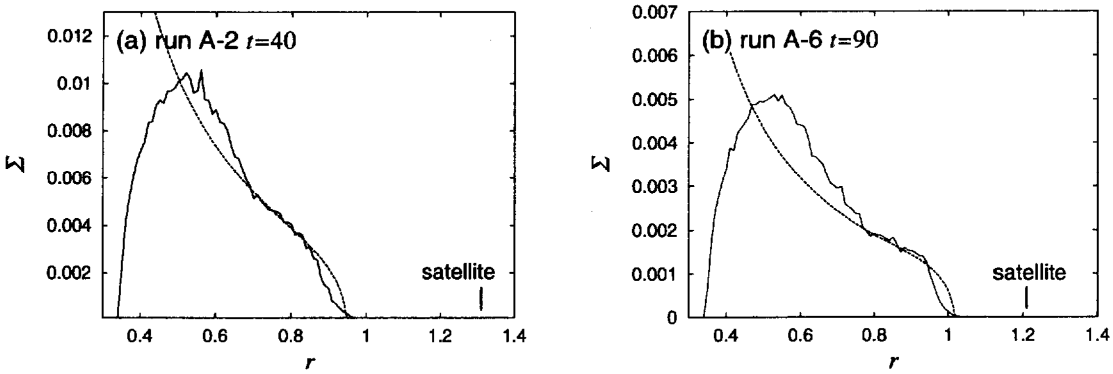

Fig. 10.— Solid line is surface density distribution defined by semimajor axis of particles, and dotted line is surface density estimated by eq. (62). Panel (a) is for run A-2 at $t = 40$ and (b) is for run A-6 at $t = 90$.

4.3.4. Gap width and satellite mass

In this subsection, we determine the relation between the satellite mass and disk surface density. Equations. (59) and (62) show that Σ vanishes at $r = r_{\rm eq}$, where $r_{\rm eq}$ is defined by

$$r_{\rm s} - r_{\rm eq} = \left(\frac{2\epsilon}{81C}\right)^{1/3} \left(\frac{M_s}{\pi r_{\rm s}^2 \Sigma^*}\right)^{2/3} r_{\rm s}. \tag{63}$$

As long as eq. (52) is valid, $r_{\rm eq}$ expresses the radius of disk edge.

If $b = r_{\rm s} - r_{\rm eq} \lesssim 2.5 h r_{\rm s}$, the satellite-disk interaction is attractive but not repulsive. Hence, the satellite torque no longer equilibrates with the viscous torque. Gap is not formed in this case. In other words, the condition for gap formation is

$$r_{\rm s} - r_{\rm eq} = 2.5 h r_{\rm s} = 2.5 \left(\frac{M_{\rm s}}{3M_c}\right)^{1/3} r_{\rm s}. \tag{64}$$

The distance between $r_{\rm s}$ and $r_{\rm eq}$ increases as the satellite mass increases and the disk surface density decreases as shown in eq. (63). When $M_{\rm s}$ exceeds some critical value, gap is formed. From eq. (63) and eq.(64), the critical satellite mass $M_{\rm s}$ is given by

$$M_{\rm s} = X \left(\frac{\Sigma^* \pi r_{\rm s}^2}{M_{\rm c}}\right)^2 M_{\rm c}, \tag{65}$$

where

$$X = (2.5)^3 \left(\frac{27C}{2\epsilon}\right). \tag{66}$$

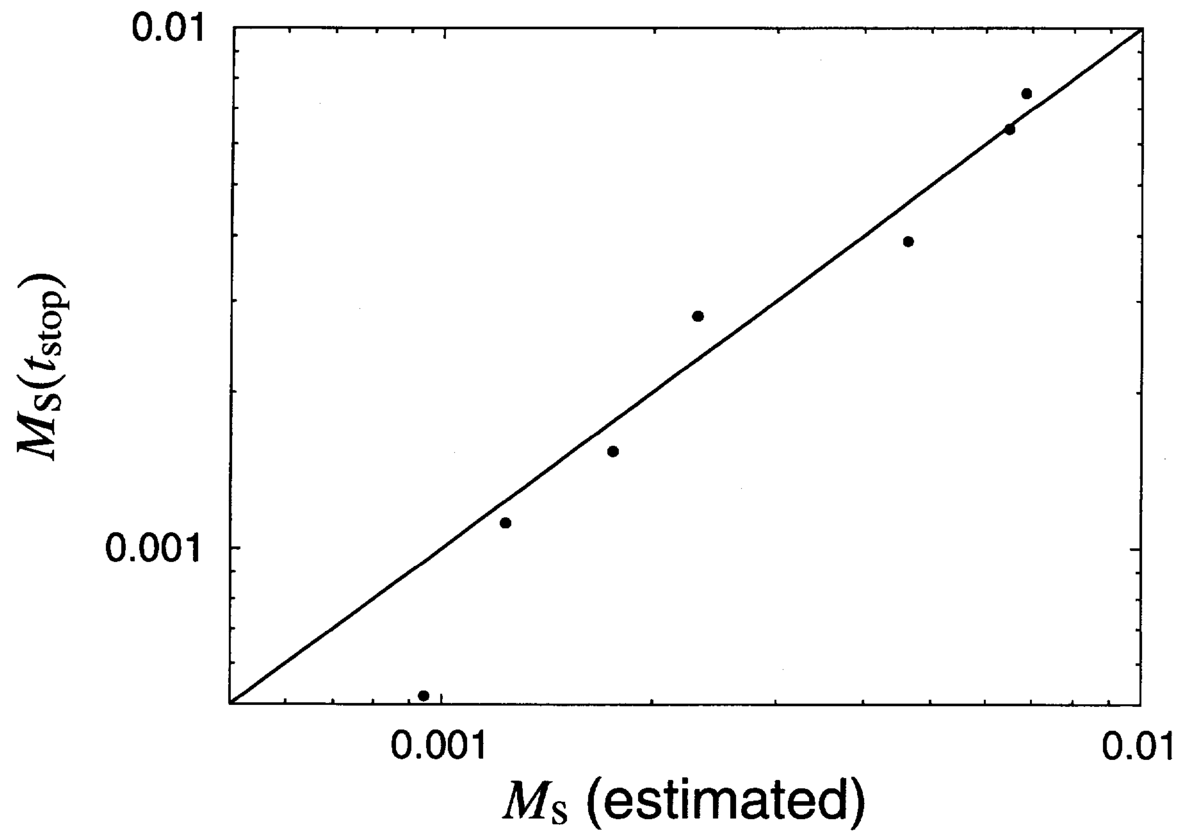

Fig. 11.— The relation between M_s in numerical simulations, and M_s estimated by eq. (65), with Σ^* evaluated from the numerical simulations. A solid line show a line at which both M_s are equal.

So far Σ^* has been a constant of integration. In the below, we analytically evaluate Σ^*. Before that, we confirm eq. (65) with Σ^* obtained by fitting the result of N-body simulation with eq. (62). We compare satellite mass $M_s(t_{stop})$ and M_s estimated by eq. (65) with the numerically derived Σ^* at t_{stop}. In Fig. 11, we show the result. Horizontal axis is M_s estimated by eq. (65), and vertical axis is $M_s(t_{stop})$ in the numerical simulation. Filled circles are results of runs of set A. Solid line show the line at which both M_s are equal. If eq. (65) is valid, circles should be along the line. Numerical results and estimations are in good agreement, indicating that eq. (65) is valid. One circle near $M_s = 0.01$ is apart from the line exceptionally. In this run (A-7), a large aggregate with considerable mass is formed in a horse shoe orbit of the satellite. If we add the mass of this aggregate to $M_s(t_{stop})$, the circle becomes to be along the line.

Now we analytically evaluate Σ^*. As shown in eq. (62), $\Sigma = \Sigma^*(r/r_s)^{-5/3}$ in the region far from r_s. Approximating this Σ distribution holds in the entire disk from r_{in} to r_{edge}, the mass of the disk is

$$M_{disk} = 2\pi\Sigma^* r_s^{5/3} \int_{r_{in}}^{r_{edge}} r^{-2/3} dr = B\pi r_s^2 \Sigma^*, \tag{67}$$

where

$$B = 6\left\{\left(\frac{r_{edge}}{r_s}\right)^{1/3} - \left(\frac{r_{in}}{r_s}\right)^{1/3}\right\}, \tag{68}$$

and

$$r_{edge} \sim \left[1 - 2.5\left(\frac{M_s}{3M_c}\right)^{1/3}\right] r_s. \tag{69}$$

Substituting eq. (67) into eq. (65), we obtain M_s as a function of M_{disk},

$$M_s = X\left(\frac{M_{disk}}{BM_c}\right)^2 M_c. \tag{70}$$

Since we need to derive M_s as a function of M^0_{disk} and l^0_{disk}, we substitute eq (70) into eqs. (44) and (45). In eq. (45), l_{disk} is given by

$$l_{disk} = \left(\frac{2\pi\Sigma^*}{M_{disk}}\right) r_s^{5/3} \int_{r_{in}}^{r_{edge}} \sqrt{GM_c} r^{-1/6} dr = \frac{2}{5}\sqrt{GM_c}\left(\frac{r_{edge}^{5/6} - r_{in}^{5/6}}{r_{edge}^{1/3} - r_{in}^{1/3}}\right). \tag{71}$$

The equation which gives the relation between M_s and M^0_{disk} and l^0_{disk} is

$$(l_s - l_{fall})^2\left(\frac{M_s}{M_c}\right)^2 - \left[2(l_s - l_{fall})Y_1 + (l_{disk} - l_{fall})^2 X^{-1} B^2\right]\left(\frac{M_s}{M_c}\right) + Y_1^2 = 0, \tag{72}$$

where

$$Y_1 = (l^0_{disk} - l_{fall})\left(\frac{M^0_{disk}}{M_c}\right). \tag{73}$$

In the limit that M^0_{disk}/M_c and M_s/M_c are small, eq. (72) becomes a simple quadric:

$$(l_{disk} - l_{fall})^2 X^{-1} B^2 \left(\frac{M_s}{M_c}\right)_{limit} = (l^0_{disk} - l_{fall})^2\left(\frac{M^0_{disk}}{M_c}\right)^2. \tag{74}$$

Thus,

$$(M_s)_{limit} = XB^{-2}\left(\frac{l^0_{disk}/l_{fall} - 1}{l_{disk}/l_{fall} - 1}\right)^2\left(\frac{M^0_{disk}}{M_c}\right)^2 M_c. \tag{75}$$

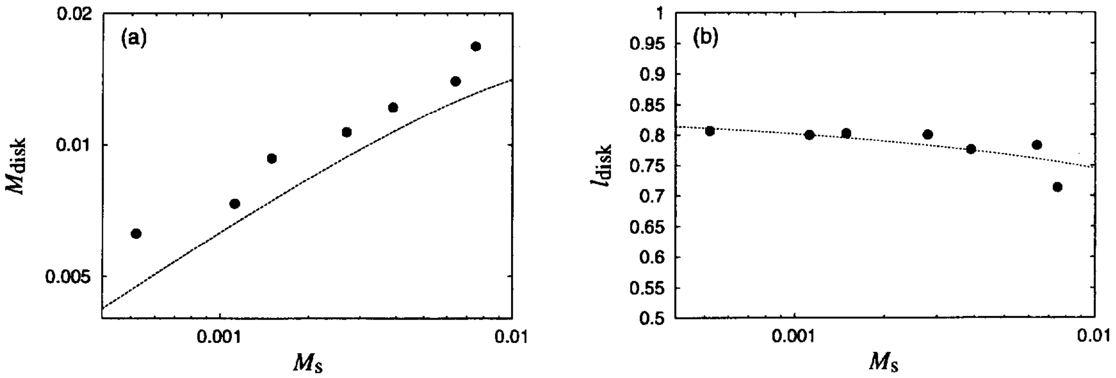

Fig. 12.— Panel (a) shows the relation between satellite mass M_s and disk mass M_{disk} at $t = t_{stop}$. Filled circles represent numerical results. Dotted line is estimated M_{disk} by eq. (70) Panel (b) shows specific angular momentum of the remaining disk at $t = t_{stop}$. Filled circles represent numerical results. Dotted line is estimated l_{disk} by eq. (71).

In this case, r_{edge} in l_{disk} [eq. (71)] is r_s. As M^0_{disk} decreases, M_s decreases with $(M^0_{disk})^2$, while M_s^{IDA97} is proportional to M^0_{disk}.

We compare the above formulae with numerical results of runs of set A. Fig. 12 (a) shows M_{disk} in numerical simulations at $t = t_{stop}$ and M_{disk} given by eq. (70) with $r_s = 1.25$ and $r_{in} = 0.35 R_R \sim R_c$. In panel (b), we show l_{disk} of numerical simulations at $t = t_{stop}$ and l_{disk} given by eq. (71). Here, numerical l_{disk} are calculated by all particles in the region $r < a[1 - 2(M_s/3M_c)^{1/3}]$, where we chose a factor 2 since it is greater than 1 and smaller than 2.5. They show good agreement. Note that we assumed that $\Sigma \propto r^{-5/3}$ in this section. In numerical simulations, viscosity C has r dependency and surface density distribution is steeper than $\Sigma \propto r^{-5/3}$ (Figs. 10), while Σ decrease near the planet's surface. As a whole, the estimation slightly underestimate M_{disk}. The difference of l_{disk} is smaller since outer region has larger weight of angular momentum than mass.

In Fig. 13, we compare the relation between final satellite mass and M^0_{disk} in the numerical simulations, and M_s given by eq. (72). We show the results of runs with initial surface density with $l^0_{disk} \sim 0.78$ (runs A-1 to A-7, and runs B-1 to B-5). We assumed that satellite is formed at $r_s = 1.25 R_R$ and particles falls to the central planet have semimajor axes $r = R_c$. Then, l_s and l_{fall} are 1.12 and 0.59 in a unit of $\sqrt{GMR_R}$. Substituting these factors to eq. (72) and solving it, we obtain M_s as a function of M^0_{disk}. A solid

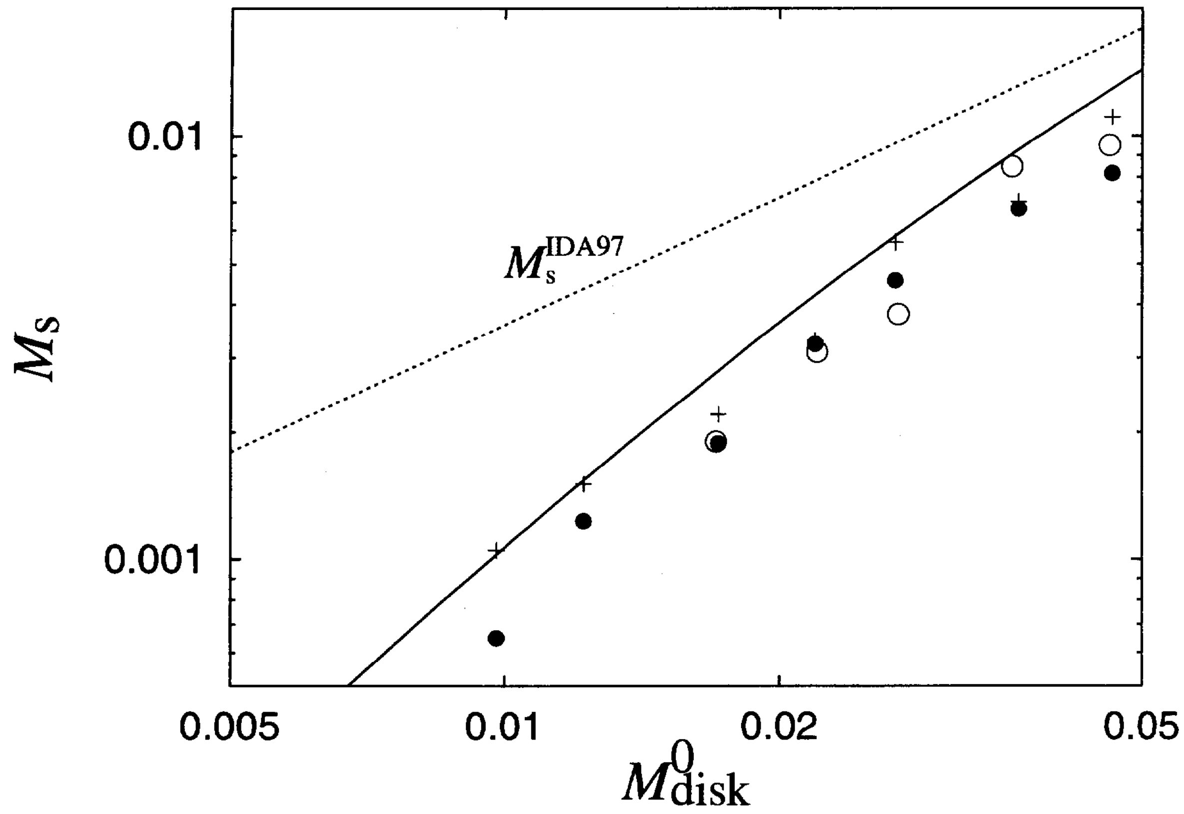

Fig. 13.— The relation between $M^0_{\rm disk}$ and $M_{\rm s}$. Filled circles show $M_{\rm s}$ of runs A, and open circles are $M_{\rm s}$ of runs B. We used $M^{-\infty}_{\rm disk}$ instead of $M^0_{\rm disk}$ for runs B. $M_{\rm s}$ are values at the end of simulations, which is slightly larger than $M_{\rm s}$ at $t = t_{\rm stop}$ (Fig. 9 (a)). Crossed points indicate the sum of the mass of satellite and second largest aggregates, which is in horse shoe orbit or outside the orbit of the largest satellite. Dotted line shows the satellite mass evaluated with eq. (46).

line represents $M_{\rm s}$ given by eq. (72). Filled and open circles are result of runs of sets A and B. In some runs of set A, an aggregate with considerable mass is in horse shoe orbit or outside the orbit of the satellite. We also show the sum of the mass of satellite and second largest aggregate by crossed points. The results of runs B and runs A (runs with and without an artificial satellite seed) are similar. The numerical results and eq. (72) show good agreement. As a comparison, we also show $M_{\rm s}^{\rm IDA97}$ given by eq. (46) by a dashed line. In the case with $M^0_{\rm disk}$ appropriate to protolunar disk ($M^0_{\rm disk} \gtrsim 0.04 M_{\rm c}$), difference between eq (72) and eq.(46) is small. However, $M_{\rm s}$ given by eq. (72) is always

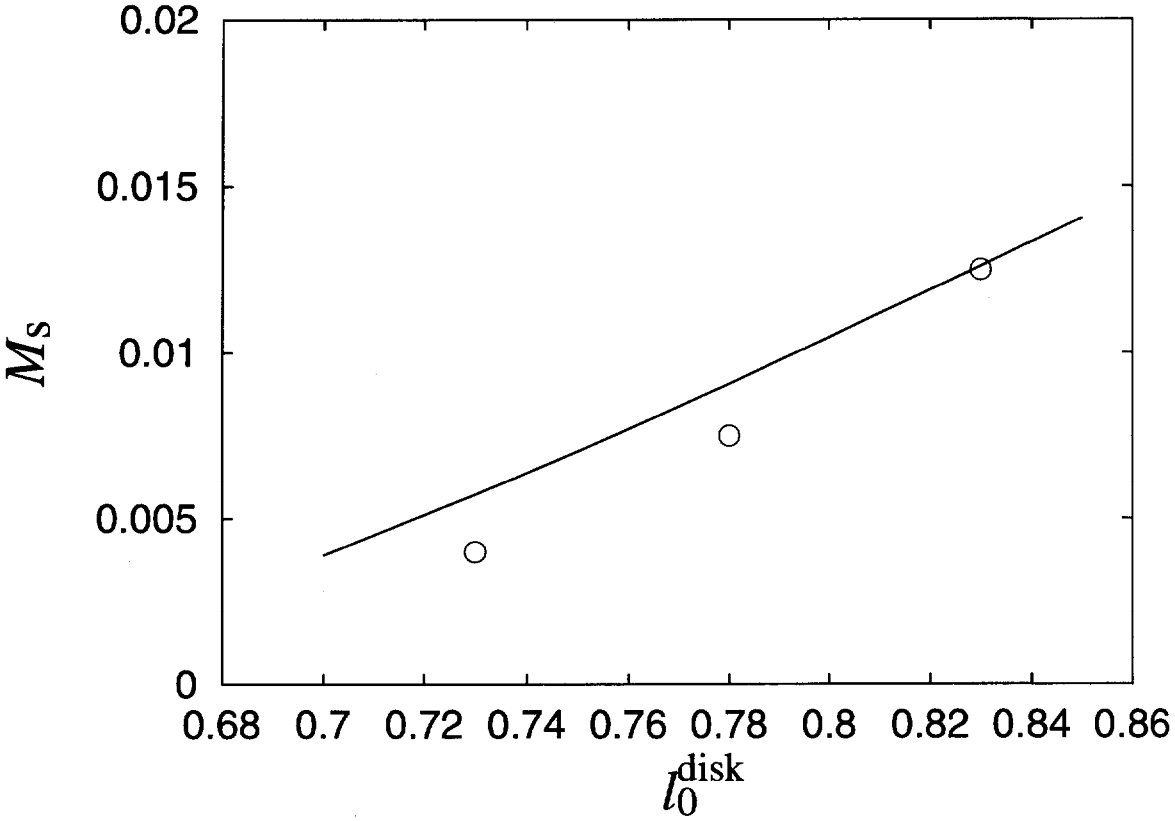

Fig. 14.— The relation between $l^0_{\rm disk}$ and $M_{\rm s}$. Open circles show $M_{\rm s}$ of runs B-2, B-9 and B-10.

smaller than $M_{\rm s}^{\rm IDA97}$, since some fraction of mass remains in the disk.

We also compare the relation between satellite mass and $l^0_{\rm disk}$. In Fig. 14, we show the dependency of $M_{\rm s}$ on $l^0_{\rm disk}$. Runs B-2, B-9 and B-10 have a same $M_{\rm disk}^{-\infty} = 0.036M_{\rm c}$, while they have different $l^0_{\rm disk} = 0.78$, 0.73 and 0.83 respectively. Here, $M_{\rm disk}^{-\infty}$ is disk mass including the existence of artificial satellite seed (see section 5.2). A solid line represents $M_{\rm s}$ given by eq. (72), and filled circles represent $M_{\rm s}$ in numerical simulations. They are in agreement.

The mass $M_{\rm s}$ in numerical results are somewhat smaller than eq. (72) systematically. Some of this would come from the neglection of particles which escape from the system, and that we do not include the mass or particles scattered outside the Roche limit but not accreted to the satellite.

Table 2. satellite mass and disk mass at the stopping time

RUN	$M_{\rm disk}^{0,-\infty}$	$M_{\rm s,1}$	$M_{\rm s,2}$	$M_{\rm disk}$
RUN A-1	0.046	0.0075	-	0.0168
RUN A-2	0.037	0.0064	-	0.0140
RUN A-3	0.027	0.0039	-	0.0122
RUN A-4	0.022	0.0028	-	0.0111
RUN A-5	0.017	0.00154	-	0.0095
RUN A-6	0.012	0.00117	-	0.00753
RUN A-7	0.0098	0.00052	-	0.00627
RUN B-1	0.046	0.0085[a]	-	-
RUN B-2	0.036	0.0075[a]	-	-
RUN B-3	0.027	0.0038[b]	0.00124	0.0051
RUN B-4	0.022	0.0031[b]	0.00118	0.0041
RUN B-5	0.017	0.0018[b]	0.00094	0.0061
RUN B-6	0.075	0.0154[a]	-	-
RUN B-7	0.060	0.0111[a]	-	-
RUN B-8	0.048	0.0075[a]	-	-
RUN B-9	0.036	0.0040[b]	0.00142	0.0072
RUN B-10	0.036	0.0125[a]	-	-
RUN B-11	0.024	0.0069[a]	-	-
RUN B-12	0.017	0.0042[a]	-	-

[a] $M_{\rm s,1}$ at the end of the simulation

[b] $M_{\rm s,1}$ just before the formation of the secondary satellite

Table 3. Notations

Notation	Meaning
M_{c}	Mass of the central planet
M^0_{disk}	Mass of the debris disk at $t = 0$
M_{disk}	Mass of the debris disk
$M^{-\infty}_{\mathrm{disk}}$	Mass of the initial debris disk, introduced in the runs with artificial satellite seed (see section 5.2)
$M^{\mathrm{crit}}_{\mathrm{disk}}$	Critical disk mass for the formation of secondary satellite
M_{fall}	Cumulative mass that falls to the central planet
M_{s}	Mass of the satellite
M^0_{s}	Initial mass of the artificial satellite seed
$M_{\mathrm{s},k}$	Mass of the k-th satellite
l^0_{disk}	Specific angular momentum of the debris disk at $t = 0$
l_{disk}	Specific angular momentum of the debris disk
l_{fall}	Specific angular momentum of materials which fall to the central planet
l_{s}	Specific angular momentum of the satellite
$l_{\mathrm{s},k}$	Specific angular momentum of the k-th satellite
R_{R}	radius of Roche limit
R_{c}	Radius of the central planet
r_{s}	Semimajor axis of the satellite
$r_{\mathrm{s},k}$	Semimajor axis of the k-th satellite
r_{edge}	Location of the disk edge
T_{K}	Kepler time at $r = R_{\mathrm{R}}$
t_{stop}	Time at which the growth of the satellite stops
t_{mig}	Time at which the outward migration of the satellite begins
t_{grow}	Time at which the rapid growth of the satellite begins

5. THE CONDITION FOR SECONDARY SATELLITE FORMATION

In this section, we describe the orbital evolution of a primary satellite, and formation of a secondary satellite. Finally, using the relation between the disk mass and satellite mass discussed in previous section, we derive a condition for the formation of multiple satellite system, and compare them with numerical results.

5.1. Migration of a Primary Satellite and Formation of a Secondary Satellite

5.1.1. Migration of a primary satellite and increase of gap width

A primary satellite migrates outward after $t_{\rm mig}$. Since viscous torque and satellite torque are in equilibrium, increase of angular momentum of the satellite is equal to the viscous angular momentum flux given by eq.(49). Thus, increase of specific angular momentum is

$$\frac{dl_{\rm s}}{dt} \sim \frac{\pi^3 G^2}{\Omega^2} r^2 \Sigma^3 M_{\rm s}^{-1}. \tag{76}$$

Using the relation $dl_{\rm s}/dt = (1/2) r_{\rm s}\Omega_{\rm s}(dr_{\rm s}/dt)$, replacing Σ by $\Sigma^*(r/r_{\rm s})^{-5/3}$, and substitute eq. (65) to eq. (76), the migration rate is

$$\frac{dr_{\rm s}}{dt} \sim 2X^{-1}\left(\frac{\pi r_{\rm s}^2\Sigma^*}{M_{\rm c}}\right) r_{\rm s}\Omega_{\rm s}. \tag{77}$$

Since $M_{\rm disk}$ is proportional to Σ^*, (eq, (67)), the time scale of migration of satellite $r_{\rm s}/(dr_{\rm s}/dt)^{-1}$ is proportional to $M_{\rm disk}^{-1}$. On the other hand, time scale of the diffusion of the disk is proportional to Σ^{-2} (eq. (42)), i.e. proportional to $M_{\rm disk}^{-2}$. The time scale of migration of the satellite is faster than the time scale of diffusion in a less massive disk. This is because satellite-disk mass ratio decreases as disk mass decreases. Thus, the gap width between the disk and satellite increases.

Then, we consider the maximum gap width. Torque from a satellite on a disk is deposited at resonance radii (Goldreich & Tremaine 1980). In the vicinity of the satellite, there are many $m : m-1$ resonances. Note that eq. (52) can be obtained by averaging interactions of many resonances in the vicinity of the satellite (Goldreich

& Tremaine 1980). However, these resonances become sparse as the distance from the satellite increases, and beyond the 2:1 resonance at $r = 0.63r_s$, there is no $m : m-1$ resonance. Thus, disk-satellite interaction decreases drastically if $r_{edge} < 0.63r_s$. When the maximum gap width is achieved, the disk edge comes to be about $0.63r_s$. In the parameter range of our simulations, this relation is achieved (see Figs. 5). Also, the negative angular momentum deposited at resonance tends to pile up particles near the resonance (Figs. 6 panel (b)). Goldreich & Tremaine (1978) pointed out that this mechanism would encourage the formation of another satellite and may account for the formation of resonant pairs of satellites. As shown below, satellites formed in our simulations are locked to 2:1 resonance relation immediately after the formation of a secondary satellite.

5.1.2. Formation of secondary satellite

We show the evolution of semimajor axes and masses of the primary and the secondary satellites of in Figs. 15. Panels (a) and (b) show semimajor axes of the primary satellite in runs B-1 and B-2. In these runs, the disks do not have enough mass to repel the primary satellite enough, and disk remains within the Roche limit and the formation of a secondary satellite does not occur. Panels (c) and (d) show semimajor axes of satellites in runs B-3 and B-4, and panels (e) and (f) show mass growth of satellites in the same runs. When r_s reaches about $1.8R_R$, formation of a secondary satellite begins. Initially, a secondary satellite grows rapidly. After a gap is formed between the secondary satellite and the disk, the growth of the secondary satellite slows down and outward migration of the satellite begins.

We also give secondary satellite mass $M_{s,2}$ and disk mass M_{disk} at stopping time $t_{stop,2}$ in Table 2. To be consistent with t_{stop} of a primary satellite, stopping times $t_{stop,2}$ are determined as $t_{stop,2} - t_{grow,2} = 1.5(t_{mig,2} - t_{grow,2})$, where $t_{grow,2}$ is determined as the time that rapid growth of the secondary satellite begins. Stopping times are shown in Figs 15 (c), (d), (e), and (f) by filled circles.

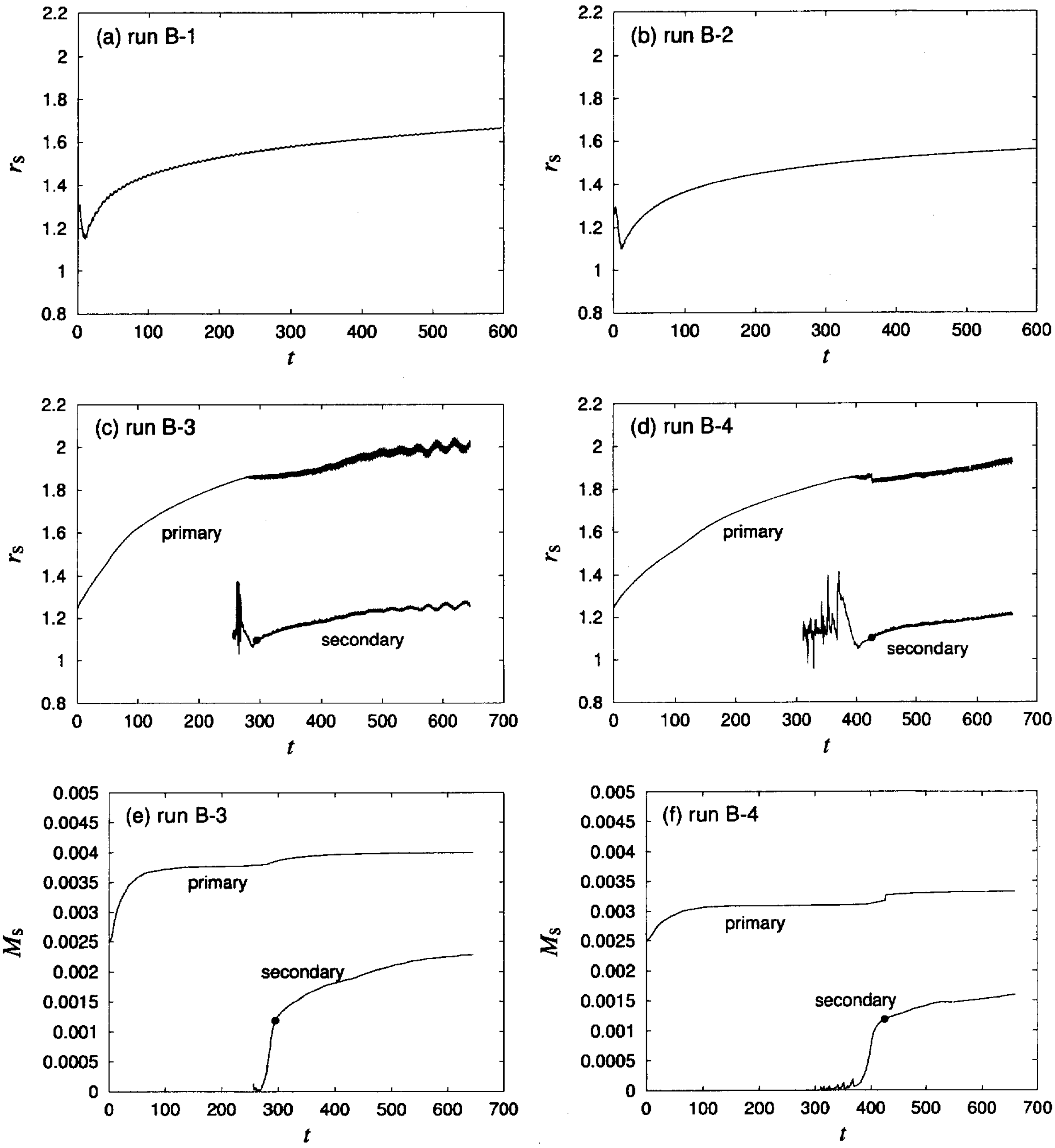

Figs. 15

Fig. 15.— Evolution of semimajor axes of the primary and the secondary satellites for runs B. Panels (a), (b), (c), and (d) are for runs B-1,2,3 and 4 respectively. Panel (e) and (f) show mass growth of the primary and the secondary satellites of runs B-3 and B-4 respectively.

5.1.3. Resonance pairs of satellites

After a secondary satellite is formed, the secondary satellite migrates outward, gaining angular momentum from the remaining disk (Figs. 15 (c) and (d)). Disk-satellite interaction decays with the distance between the satellite and the disk. Thus, disk satellite interaction between the disk and the secondary satellite, which is near the disk edge, is stronger than the interaction between the primary satellite and the disk, unless $M_{\mathrm{s},2} \ll M_{\mathrm{s},1}$. In such a system that two satellites migrate outward with different rates $d(r_{\mathrm{s},1}/r_{\mathrm{s},2})/dt < 0$, satellites fall to the m:n resonance relation when $\Omega(r_{s,2})/\Omega(r_{s,1})$ becomes m/n, unless the initial eccentricity is larger than a critical eccentricity (e.g., Peale 1986). When two satellites are locked in a resonance, a fraction of angular momentum transfered to the inner satellite from the disk is passed to the outer satellite through the resonance interaction (e.g., Peale 1986). This interaction keeps the resonance relation of two satellites. In our simulations, secondary satellite is formed near the 2:1 resonance of a primary satellite, and their orbits are locked into the resonance immediately.

The resonance relation is described by a resonant angle. We will show the evolution of resonant angles in the numerical simulations. Here, we briefly describe the meaning of resonant angle. We introduce orbital elements λ, ϖ. They are mean longitude, longitude of pericenter respectively. We consider coplanar orbits, so that longitude of ascending node is not important here. We consider configurations of satellites at every conjunction, at which $\lambda_1 = \lambda_2$. If two satellites are in resonance, they are in similar configuration at every conjunction. For example, if a secondary satellite is at its pericenter at every conjunction, the mean anomaly of the secondary satellite ($M_2 = \lambda_2 - \varpi_2$) is 0 when $\lambda_1 = \lambda_2$. The mean anomaly of satellites at every conjunction are described by resonant angles. In the case of 2:1 resonance, resonant angles are

$$\varphi_1 = 2\lambda_1 - \lambda_2 - \varpi_1, \tag{78}$$

$$\varphi_2 = 2\lambda_1 - \lambda_2 - \varpi_2. \tag{79}$$

At every conjunction ($\lambda_1 = \lambda_2$), each resonant angle is equal to the mean anomaly of each satellite:

$$\varphi_1 = \lambda_1 - \varpi_1 = M_1, \tag{80}$$

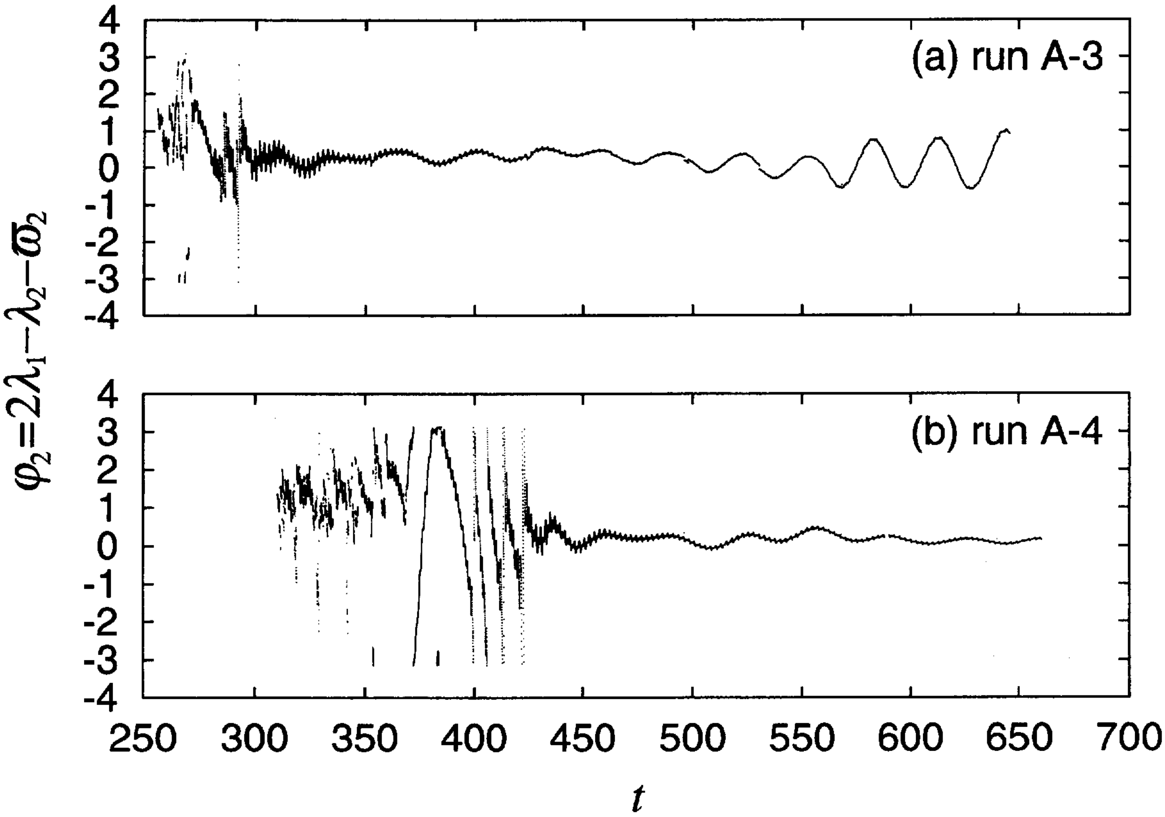

Fig. 16.— Evolutions of a resonant angle φ_2. Panel (a) is for run B-3 and panel (b) is for run B-4. In both cases, satellites are captured into 1:2 resonance soon after secondary satellite formation.

$$\varphi_2 = \lambda_2 - \varpi_2 = M_2. \tag{81}$$

If φ_1 or φ_2 is 0, two satellite are in an exact 2:1 resonance. Near the exact resonance, φ_1 or φ_2 librates around 0. In this case, satellites are in resonance relation. If φ_1 and φ_2 increase or decrease monotonically, satellites are not in resonance relation.

We show the evolution of resonance angle $\varphi_2 = 2\lambda_1 - \lambda_2 - \varpi_2$ of run A-3 and A-4 in Figs. 16. The secondary satellites are fully formed at about 300 T_K and 420 T_K respectively (see Figs. 9). Initially, the resonant angles decreases monotonically. However, soon after the secondary satellite is fully formed, resonance angle φ_2 begins to oscillate around 0, indicating that two satellites are in 2:1 resonance relation. At every conjunction, the secondary satellite is near its pericenter ($M_2 = \lambda_2 - \varpi_2 = \varphi_2 \sim 0$).

This rapid formation of a resonance pair implies that the secondary satellite is formed just inside the 2:1 resonance. This comes from that a secondary satellites is formed by particles piled up at 2:1 resonance. As mentioned above, a satellite tends to migrate somewhat inward when it is growing, so that it tends to be inside the resonance when its outer migration begins. Thus, the secondary satellite approaches the resonance from inside, and the satellite is captured to the resonance.

Through the resonance interaction, angular momentum from the disk to the secondary satellite is transfered to the primary satellite. Thus, the entire system expands after the secondary satellite formation (Figs. 15 panel (c) and (d)).

5.2. The Condition for Secondary Satellite Formation

The formation of a secondary satellite depends on whether the disk edge passes through the Roche radius again. In this section, we derive a necessary condition for secondary satellite formation, considering how far the primary satellite migrates, which is determined by the mass of the satellite and the remaining disk. As the primary satellite migrates outward, disk edge migrates outward. However, mass of the disk decreases with time, while mass of the satellite does not decrease. Satellite-disk interaction would eventually clear the remaining disk to the central planet, though it would take relatively long time to clear the disk inside 2:1 resonance (Fig. 5 panel (d)).

At first, we derive the maximum orbital radius of a primary satellite. Assuming that all disk material falls to the central planet by disk-satellite interaction, conservation laws of mass and angular momentum are written as

$$l_{\mathrm{disk}}^0 M_{\mathrm{disk}}^0 = l_{\mathrm{fall}}(M_{\mathrm{disk}}^0 - M_{\mathrm{s}}) + l_{\mathrm{s}}^{\infty} M_{\mathrm{s}}, \tag{82}$$

where l_{s}^{∞} is specific angular momentum of the primary satellite at $t = \infty$. Substituting M_{s} given by eq. (72) to eq. (82), and using the relation $l_{\mathrm{s}} = \sqrt{GM_{\mathrm{c}} r_{\mathrm{s}}}$, the final location of the primary satellite r_{s}^{∞} is given as a function of M_{disk}^0. We show the resulting r_{s}^{∞} in Fig. 17. We adopted the numerical factors $\epsilon = 14.4, C = 5, l_{\mathrm{disk}}^0 = 0.78\sqrt{GM_{\mathrm{c}} R_{\mathrm{R}}}$, and $l_{\mathrm{fall}} = 0.59\sqrt{GM_c R_R}$ as before. A solid line represents r_{s}^{∞}.

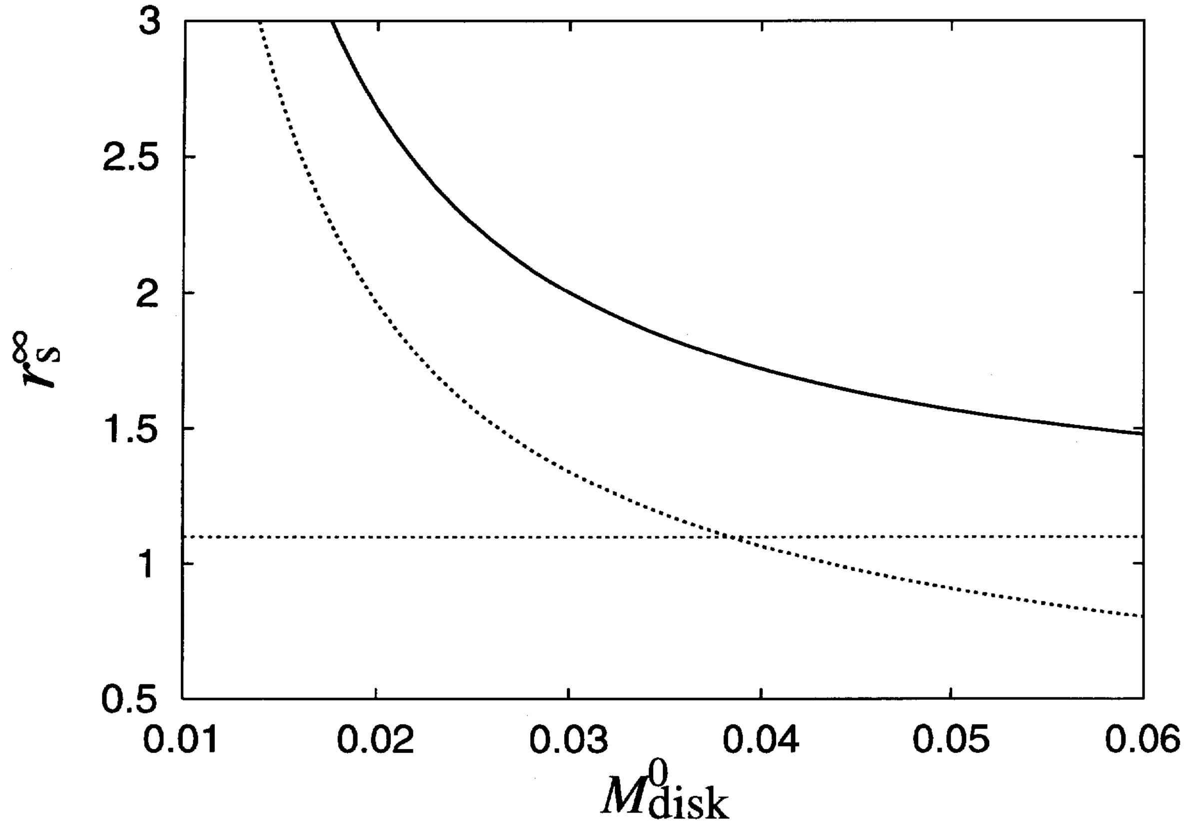

Fig. 17.— Solid line is final location of the primary satellite $r_{\rm s}^{\infty}$ given by eq. (82). Dotted line shows $r_{\rm edge}^{\rm max}$ (eq. (91)). The necessary condition for the formation of secondary satellite is that $r_{\rm edge}^{\rm max} > \beta R_{\rm R}$. Horizontal line represents $1.1 R_{\rm R}$.

Next, we consider the location of the disk edge ($r_{\rm edge}$). Gap width is initially $2.5(M_{\rm s}/3M_{\rm c})^{1/3}$ and increases. Maximum of gap width is $r_{\rm edge} \sim 0.63 r_{\rm s}^{\infty}$. Then, the maximum of $r_{\rm edge}$ is given as $r_{\rm edge}^{\rm max} = [1 - 2.5(M_{\rm s}/3M_{\rm c})^{1/3}] r_{\rm s}^{\infty}$, while minimum $r_{\rm edge}^{\rm min} = 0.63 r_{\rm s}^{\infty}$.

For the formation of secondary satellite, $r_{\rm edge}^{\rm max}$ must exceed the Roche limit. Thus, the necessary condition for secondary satellite formation is

$$r_{\rm edge}^{\rm max}[1 - 2.5(M_{\rm s}/3M_{\rm c})^{1/3}] r_{\rm s}^{\infty} > \beta R_{\rm R}, \tag{83}$$

where β express the location where secondary satellite formation becomes possible. Empirically, β = [1.1-1.25]. Since we consider necessary condition here, we adopt 1.1 for β here. We show $r_{\rm edge}^{\rm max}$ by a dotted line, while $1.1 R_{\rm R}$ by a horizontal dotted line in Fig. 17.

In this case that $l_{\rm disk}^0 = 0.78\sqrt{GM_{\rm c}R_{\rm R}}$, the secondary satellite would be formed if initial disk mass is

$$M_{\rm disk}^0 < M_{\rm disk}^{\rm crit} \sim 0.04 M_{\rm c}. \tag{84}$$

In the case of a massive disk appropriate to a protolunar disk ($M_{\rm disk}^0 \gtrsim 0.04$), $r_{\rm edge}^{\rm max} < \beta R_{\rm R}$, so that secondary satellite can not be formed from the remaining disk, being consistent with previous works of lunar accretion (Ida, Canup & Stewart 1997; Kokubo, Ida & Makino 2000). Note that eq. (84) is a necessary condition for secondary satellite formation, so that true $M_{\rm crit}$ would be somewhat smaller. However, eq. (84) is a good approximation. This is because $M_{\rm s}$ decreases with decreasing $M_{\rm disk}^0$ so that $r_{\rm s}^{\infty}$ increases rapidly as $M_{\rm disk}^0$ decreases. And also, the difference between $r_{\rm edge}^{\rm max}$ and $r_{\rm edge}^{\rm min}$ is small when $M_{\rm disk}^0 \sim M_{\rm disk}^{\rm crit}$, so that the choice of $r_{\rm edge}^{\rm max}$ does not matter much.

We can similarly evaluate $M_{\rm disk}^{\rm crit}$ for different $l_{\rm disk}^0$. We show $M_{\rm disk}^{\rm crit}$ as a function of $l_{\rm disk}$ in Fig. 18 (solid line), and we compare $M_{\rm disk}^{\rm crit}(l_{\rm disk}^0)$ with the numerical results.

Before that, we must introduce initial disk mass $M_{\rm disk}^{-\infty}$ including mass of satellite seed, since we put an artificial satellite seed in runs B. Assuming that a disk with $M_{\rm disk}^0$ and satellite seed of mass $M_{\rm s}^0$ are formed from a primal disk with mass $M_{\rm disk}^{-\infty}$, the conservation laws of mass and angular momentum are $M_{\rm disk}^{-\infty} = M_{\rm fall}^0 + M_{\rm disk}^0 + M_{\rm s}^0$, and $l_{\rm disk}^{-\infty} M_{\rm disk}^{-\infty} = l_{\rm fall}^0 M_{\rm fall}^0 + l_{\rm disk}^0 M_{\rm disk}^0 + l_{\rm s}^0 M_{\rm s}^0$. Assuming that $l_{\rm disk}^{-\infty} = l_{\rm disk}^0$, these two equations give

$$M_{\rm disk}^{-\infty} = M_{\rm disk}^0 + \left(\frac{l_{\rm s}^0 - l_{\rm fall}}{l_{\rm disk}^0 - l_{\rm fall}} \right) M_{\rm s}^0. \tag{85}$$

In our simulation, we chose such $M_{\rm disk}^0$ and $M_{\rm s}^0$ that $M_{\rm disk}^{-\infty}$ of run B-n are equal to $M_{\rm disk}^0$ of run A-n, where n is from 1 to 5 (see Table 1). We use $M_{\rm disk}^{-\infty}$ instead of $M_{\rm disk}^0$ when we compare the result of runs B with the estimations. Note that we already used $M_{\rm disk}^{-\infty}$ instead of $M_{\rm disk}^0$ for runs B in Figs. 13 and 14.

We compare the numerical result and $M_{\rm disk}^{\rm crit}$ analytically estimated. Open circles in Fig. 18 represent the runs in which two satellite system is formed, and filled circles represent the runs in which single-satellite system is formed. In the case that $M_{\rm disk}^0 \sim M_{\rm disk}^{\rm crit}$, the mass of the remaining disk becomes too small when the primary satellite migrate enough for secondary satellite formation. In this case, the number of disk particles

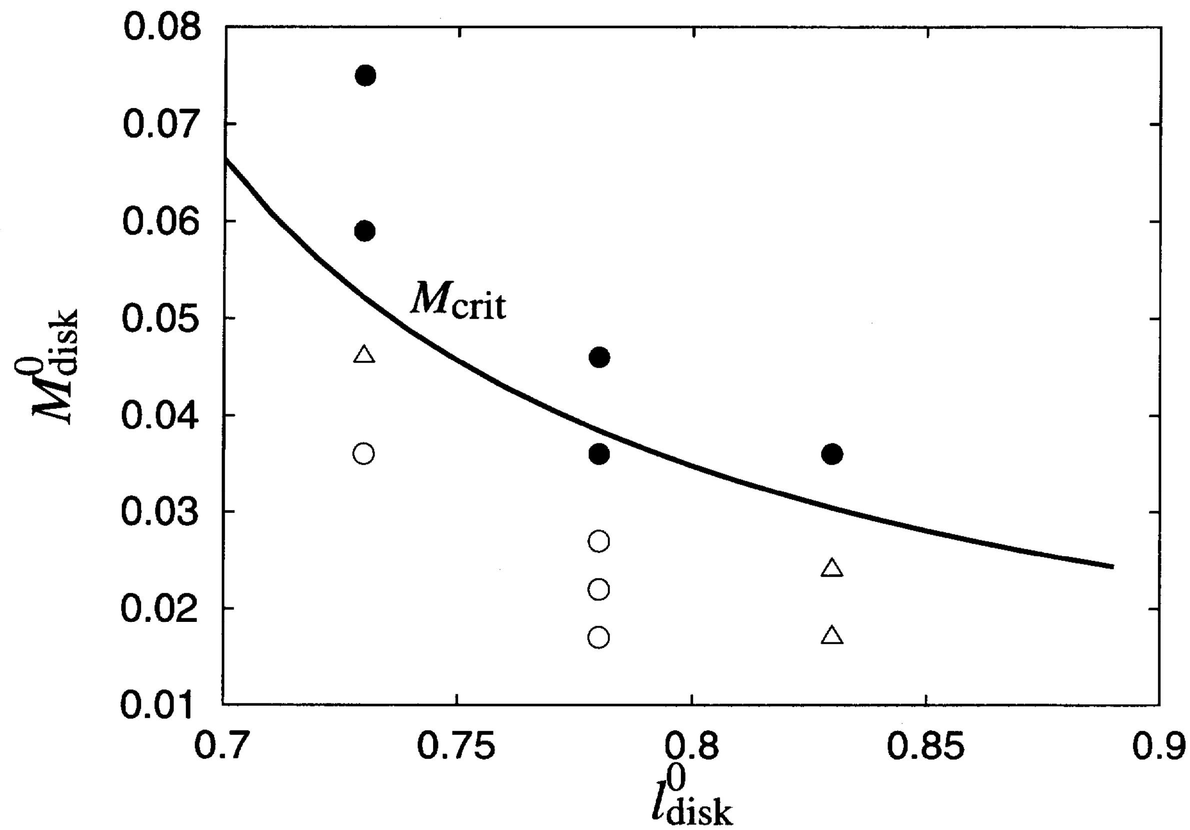

Fig. 18.— Solid line shows the critical initial disk mass $M_{\rm disk}$ as a function of $l^0_{\rm disk}$. Open circles represent the runs in which a secondary satellite is formed, and filled circles represent the runs in which a secondary satellite is not formed. Triangles represent the runs in which a primary satellite migrates up to 1.75 $R_{\rm R}$, though a secondary satellite is not formed.

becomes too small to satisfy the condition eq. (41) in the last stage of simulations, while the time scale of disk evolution becomes longer. Thus, it is somewhat difficult to determine whether a secondary satellite would be formed or not. By triangles, we denote the cases that the primary satellite reaches $1.75R_{\rm R} = (1.1/0.63)R_{\rm R}$, though an aggregate with considerable mass is not formed until $t = 2000T_{\rm K}$ in the simulation. The estimations and numerical results agree well.

5.3. Mass of a Secondary Satellite

We estimate the mass of secondary satellite in this subsection. The conservation law of mass and angular momentum are

$$M_{\rm disk}^0 = M_{\rm disk} + M_{\rm fall} + M_{\rm s,1} + M_{\rm s,2}, \tag{86}$$

$$l_{\rm disk}^0 M_{\rm disk}^0 = l_{\rm disk} M_{\rm disk} + l_{\rm fall} M_{\rm fall} + l_{\rm s,1} M_{\rm s,1} + l_{\rm s,2} M_{\rm s,2}. \tag{87}$$

The relation between disk mass $M_{\rm disk}$ and satellite mass $M_{\rm s,2}$ at $t_{\rm stop,2}$ is determined by eq. (70). Thus, the equation which determines the mass of the secondary satellite, which corresponds to eq. (72), is

$$(l_{\rm s,2} - l_{\rm fall})^2 \left(\frac{M_{\rm s,2}}{M_{\rm c}}\right)^2 - \left[2(l_{\rm s,2} - l_{\rm fall})Y_2 + (l_{\rm disk} - l_{\rm fall})^2 X^{-1} B^2\right] \left(\frac{M_{\rm s,2}}{M_{\rm c}}\right) + Y_2^2 = 0, \tag{88}$$

where X and B are given by eqs. (66) and (68) and Y_2 is

$$Y_2 = (l_{\rm disk}^0 - l_{\rm fall}) \left(\frac{M_{\rm disk}^0}{M_{\rm c}}\right) - (l_{\rm s,1} - l_{\rm fall}) \left(\frac{M_{\rm s,1}}{M_{\rm c}}\right). \tag{89}$$

The mass of the primary satellite $M_{\rm s,1}$ is given in previous sections. We assume that a secondary satellite is formed at $r_{\rm s,2} = \beta R_{\rm R}$, and $l_{\rm s,2}$ is given by $l_{\rm s,2} = r_{\rm s,2}^2 \Omega(r_{\rm s,2})$. The only unknown factor is $l_{\rm s,1} = r_{\rm s,1}^2 \Omega(r_{\rm s,1})$. This factor indicates how far the primary satellite migrates when a secondary satellite is formed.

In the previous section, we first derived $r_{\rm s}^{\infty}$, and derived $r_{\rm edge}^{\rm max}$ and $r_{\rm edge}^{\rm min}$ consequently. Here, we assume $r_{\rm edge}$ is at $\beta R_{\rm R}$, and then derive $r_{\rm s,1}$. In the limit that gap width is 2.5 $(M_{\rm s,1}/3M_{\rm c})^{1/3} r_{s,1}$, $r_{\rm s,1}$ has a minimum value:

$$[1 - 2.5(M_{\rm s,1}/3M_{\rm c})^{1/3}] r_{\rm s,1}^{\rm min} = \beta R_{\rm R}. \tag{90}$$

If we assume that the gap width increases until $r_{\rm edge}$ reaches 2:1 resonance between the primary satellite and disk edge, $r_{\rm s,1}$ has a maximum value:

$$0.63 r_{\rm s,1}^{\rm max} = \beta R_{\rm R}. \tag{91}$$

Note that if $M_{\rm s,1} > 0.0097 M_{\rm c}$, $r_{\rm s,1}^{\rm min}$ exceeds $r_{\rm s,1}^{\rm max}$.

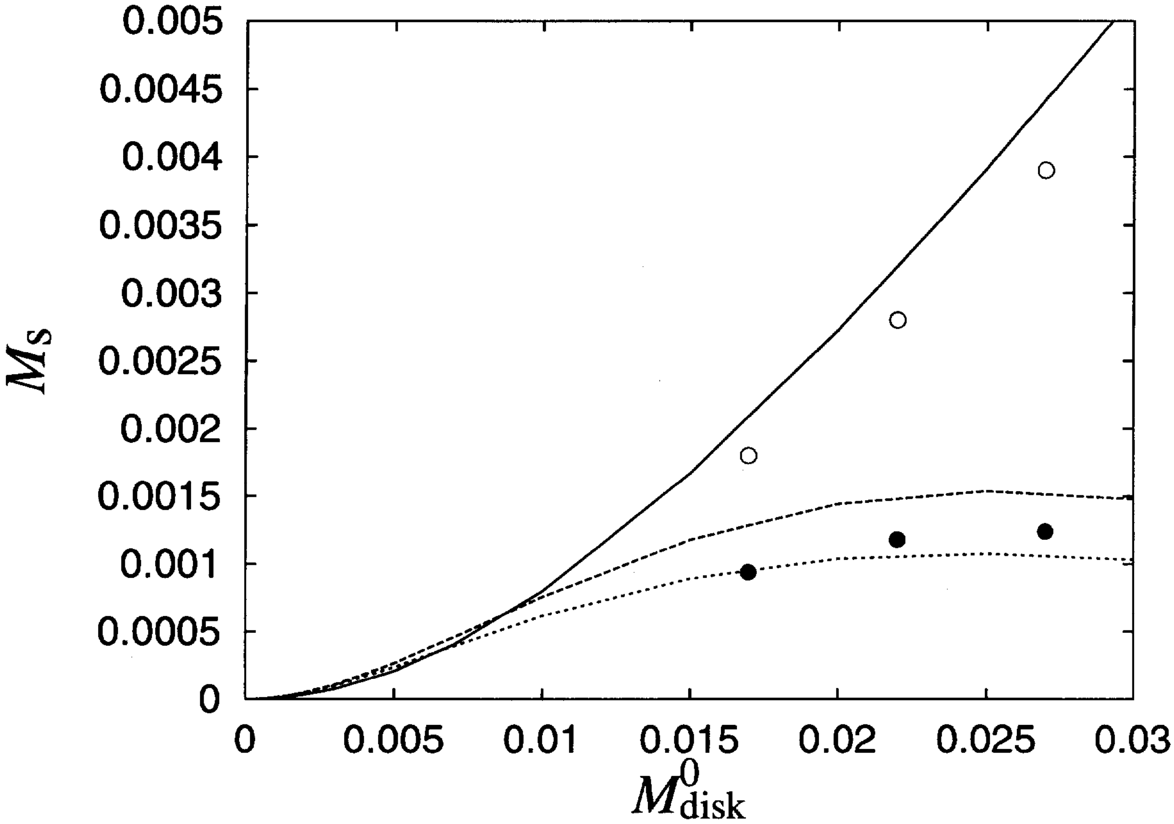

Fig. 19.— Solid lines are estimated masses of primary and secondary satellites, estimated by 75% of of eq. (72) and eq. (88). Dashed line is $M_{\rm s,2}$ estimated with $r^{\rm min}_{\rm s,1}$, and dotted line is $M_{\rm s,2}$ estimated with $r^{\rm max}_{\rm s,1}$. Open and filled circles show the mass of primary and secondary satellites respectively in numerical simulations runs B-3, B-4 and B-5.

In Fig. 19, we show the masses of satellites of runs B-3 to B-5, which are runs with $l^0_{\rm disk} = 0.78\sqrt{GM_{\rm c}R_{\rm R}}$ and a secondary satellite is formed. Empirically, β = [1.1-1.25], so that we adopt 1.175 (mean value) as β. Since $M^0_{\rm disk}$ is near $M^{\rm crit}_{\rm disk}$, $M_{\rm s,2}$ depends on $M_{\rm s,1}$ sensitively. In numerical results, $M_{\rm s,1}$ tends to be smaller than eq. (72), so that we estimate $M_{\rm s,1}$ by 75% of eq. (72). Solid line shows $M_{\rm s,1}$, given by 75% of eq. (72). Dashed line is $M_{\rm s,2}$ estimated by eq. (88) with $r^{\rm min}_{\rm s,1}$, and dotted line is $M_{\rm s,2}$ estimated with $r^{\rm max}_{\rm s,1}$. Open and filled circles are the masses of primary and secondary satellites at their stopping times in numerical simulations respectively. The mass of the secondary satellite is well predicted by eq. (88), as long as $M_{\rm s,1}$ is given properly.

An important feature is that the mass ratio between the primary satellite and the secondary satellite approaches to 1 in a less massive disk. The mass of a satellite is determined by the disk mass at the formation time of the satellite. The difference of disk mass at the formation of a primary satellite and a secondary satellite is small in the less massive disk case, leading to the formation of satellites with the similar masses. Note that the choice of $r_{\mathrm{s},1}^{\mathrm{min}}$ and $r_{\mathrm{s},1}^{\mathrm{max}}$ does not change $M_{\mathrm{s},2}$ much. This is because difference between $r_{\mathrm{s},1}^{\mathrm{max}}$ and $r_{\mathrm{s},1}^{\mathrm{min}}$ is small in the case that $M_{\mathrm{s},1}$ is large. In the case that $M_{\mathrm{s},1}$ is small, disk mass does not decrease much, so that $M_{\mathrm{s},2} \sim M_{\mathrm{s},1}$ in anyway.

6. CONCLUSION AND DISCUSSION

6.1. Conclusion

6.1.1. Multiple Moons or Single Moon ?

In this paper, we investigated the evolution of a circumplanetary debris disk, which is initially confined within the Roche limit. We have shown that whether a single satellite system, such as the Earth/Moon system or Pluto/Charon system, or a multiple satellite system is formed from the disk depends on the initial disk mass. If the proto-satellite disk is initially spread well beyond the Roche limit, multiple satellite system would be formed there. We have shown that multiple satellite system can be formed even from a disk which is centrally condensed and most of the mass is within the Roche limit. Since accretion is inhibited within the Roche limit, radial redistribution of mass is essential for satellite formation. A satellite forms with particles which are transfered beyond the Roche limit by viscous spreading, and mass of satellites are determined by balance between viscous spreading of the disk and satellite-disk interaction. We found that mass of satellite(s) formed in this way depends on disk mass as $M_{\rm s} \propto M_{\rm disk}^2$ (Fig. 7). Numerical simulations for lunar accretion process (Ida, Canup & Stewart 1997; Kokubo, Ida & Makino 2000) demonstrated that a disk which is sufficiently massive for lunar formation makes a single satellite. However, this is not the case for a less massive disk. Mass of satellite formed from the debris disk is much smaller if an initial disk is less massive. If the ratio of the satellite mass and the remaining disk mass is small enough, the disk repels the satellite outward by large distance, and the formation of another satellite occurs. In this paper, we semi-analytically derived the condition for secondary satellite formation:

$$M_{\rm disk}^0 < M_{\rm disk}^{\rm crit}, \tag{92}$$

where $M_{\rm disk}^0$ is an initial disk mass. The critical mass $M_{\rm disk}^{\rm crit}$ depends on $l_{\rm disk}^0$, which is initial specific angular momentum of the disk (Fig. 18). The critical mass $M_{\rm disk}^{\rm crit}$ decreases as $l_{\rm disk}^0$ increases. We carried out N-body simulations with various $M_{\rm disk}^0$ and $l_{\rm disk}^0$. Numerical simulation show a good agreement with above condition.

6.1.2. Orbital resonance

We investigated satellite forming process from an initially confined disk. From such a disk, satellites are formed from inside, and they migrate outward in turn due to an interaction with a remaining disk. Satellites formed in this way migrates by large distance if initial disk is not so massive as the plotolunar disk. If another satellite exists outside, their orbits would be captured into resonance. In our simulations, all satellite pairs are in 2:1 resonance relation. This is because a primary satellite wipes disk material up to 2:1 resonance, and a secondary satellite is formed by the material piled up there. Satellite-disk interaction may account for existence of many satellites pairs in resonance in the solar system.

6.2. Evolution of a further less massive disk

In our simulation range, a third satellite with considerable mass would not be formed since mass of the remaining disk is too small compared with primary and secondary satellites. However, in the case of a further less massive disk, mass of primary and secondary satellites would be further smaller [$\propto (M^0_{\rm disk})^2$]. If disk mass remains enough compared with primary and secondary satellites, it would repel the secondary satellite enough, and the formation of third and forth satellites would be possible.

Difference between secondary satellite formation and third satellite formation lies in the existence of a primary satellite outside the secondary satellite. For the third satellite to be formed, both primary and secondary satellites must be pushed away outward enough. (Here we assumed that both satellites are in stable orbits, and that the outer satellite migrates together as the inner satellite is pushed away from the disk). Thus, condition for the formation of the third satellite is harder than eq. (84), and the formation of the fourth satellite is further harder. Finally, all disk mass would fall to the central planet and satellite formation would stop.

In this subsection, we extrapolate our results to further less massive disks. We neglect orbital evolution due to tidal effect between the satellites and the central planets

(Canup, Levison, & Stewart 1999), which could be important, because disk evolution is slow in a less massive disk. Inclusion of the tidal evolution is a future issue.

6.2.1. Successive formation of satellites

The mass of n-th satellite can be estimated by repeating the procedure similar to section 5.3 successively. Conservation laws of mass and angular momentum should be

$$M_{\rm disk}^0 = M_{\rm disk} + M_{\rm fall} + \sum_{k=1}^{n} M_{{\rm s},k}, \tag{93}$$

$$l_{\rm disk}^0 M_{\rm disk}^0 = l_{\rm disk} M_{\rm disk} + l_{\rm fall} M_{\rm fall} + \sum_{k=1}^{n} l_{{\rm s},k} M_{{\rm s},k}, \tag{94}$$

where subscript k denotes the k-th satellite. Specific angular momentum of n-th satellite is given by $r_{{\rm s},n}^2 \Omega(r_{{\rm s},n})$, as before (section 5.3), and masses of outer satellites $M_{{\rm s},k}(k = 1, 2, ..., n-1)$ are given. Then, the mass of n-th satellite is given by eq. (88), modifying Y_2 to Y_n, which is given as

$$Y_n = (l_{\rm disk}^0 - l_{\rm fall}) \left(\frac{M_{\rm disk}^0}{M_{\rm c}} \right) - \sum_{k}^{n-1} (l_{{\rm s},k} - l_{\rm fall}) \left(\frac{M_{{\rm s},k}}{M_{\rm c}} \right). \tag{95}$$

To evaluate $l_{{\rm s},k}(k = 1, 2, ..., n-1)$, we here assume that outer satellites are pushed away through the resonance interactions. Then $\Omega_{{\rm s},k}/\Omega_{{\rm s},k+1}$ remains constant. Consequently, $l_{{\rm s},k}/l_{{\rm s},k+1}$ and $r_{{\rm s},k}/r_{{\rm s},k+1}$ remain constant. With this assumption, the evolution of $r_{{\rm s},k}$ can be calculated in each step. Thus $M_{{\rm s},k}$ and $r_{{\rm s},k}$ can be calculated successively until the disk mass becomes 0.

In the following discussion, we assume that $r_{{\rm s},n-1}$ and n-th satellite are in 2:1 orbital resonance. Fig. 20 shows the resulting satellite system, with $l_{\rm disk}^0 = 0.78\sqrt{GM_{\rm c}R_{\rm R}}$. The unit of distance if $R_{\rm R}$. Panels (a), (b) and (c) show results for $M_{\rm disk}^0 = 0.03, 0.01$, and $0.003 M_{\rm c}$ respectively. Note that the adjacent satellites are in 2:1 resonance relation, which comes from the above assumption. From a debris disk with $M_{\rm disk}^0 \gtrsim 0.03 M_{\rm c}$, only one large satellite is formed, though a secondary satellite with $M_{{\rm s},2} \ll M_{{\rm s},1}$ could be formed. This is consistent with the fact that planets with a large satellite $M_{\rm s} \gtrsim 0.01 M_{\rm c}$

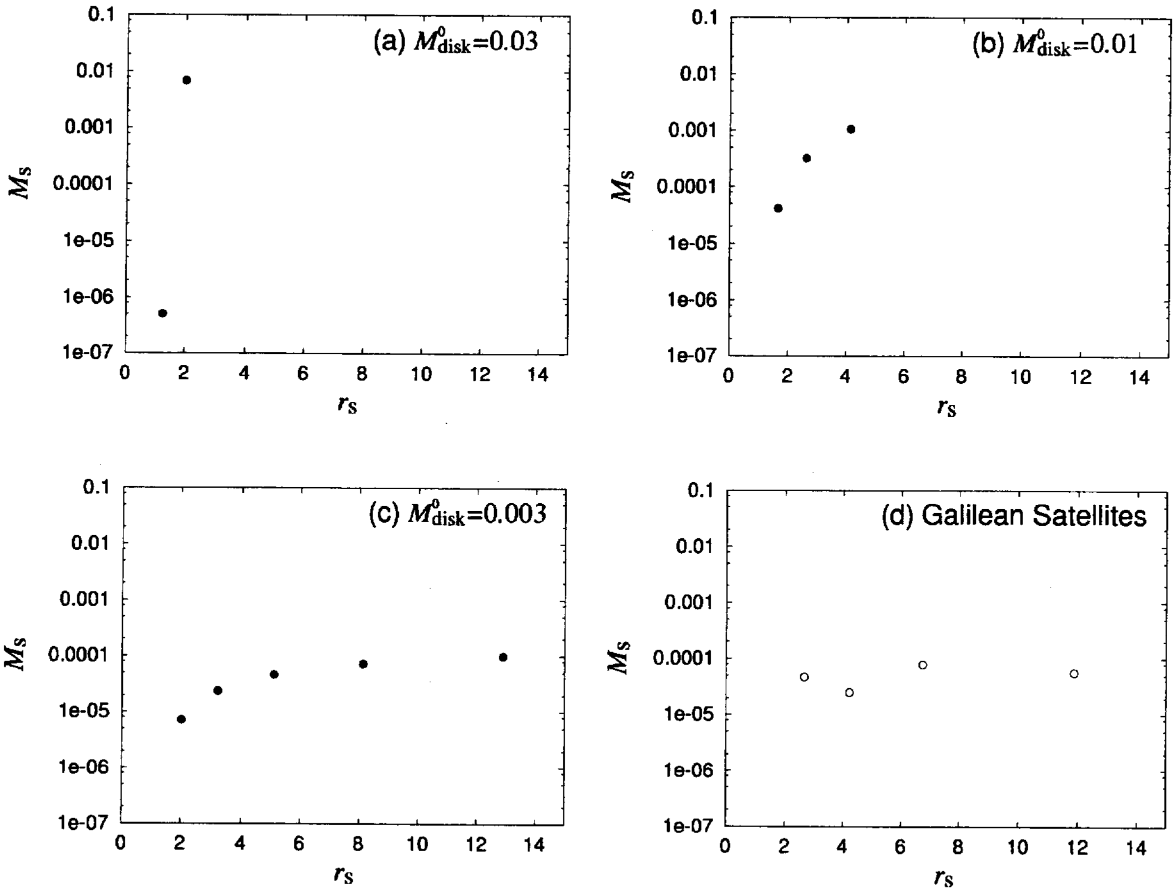

Fig. 20.— Estimated final state of the disk with $l^0_{\rm disk} = 0.78\sqrt{GM_{\rm c}R_{\rm R}}$. Panel (a), (b) and (c) show results for $M^0_{\rm disk} = 0.03, 0.01$, and $0.003M_{\rm c}$ respectively. Panel (d) shows the Galilean satellites of the Jupiter.

has only one satellite (Earth/Moon system and Pluto/Charon system). From a debris disk with $M^0_{\rm disk} \sim 0.003M_{\rm c}$, four or five satellites with mass of order of 10^{-4}-$10^{-5}M_{\rm c}$ are formed. We compare this satellite system with Galilean satellites in Jovian system as a sample of multiple satellite system. Masses of Galilean satellites are 10^{-4}-$10^{-5}M_{\rm c}$, and their number is 4. We show the four satellites of Jupiter (Io, Europa, Ganymede, and Callisto) in Panel (d). Panel (d) is scaled by $R_{\rm R}$ as well as panel (a)-(c). Here we used the relation $R_{\rm J} \sim 0.45R_{\rm R}$, assuming $\rho \sim 2$ for Jovian system. Note that Io-Europa pair and Europa-Ganymede pair are actually in 2:1 resonances respectively, which means that $r_{{\rm s},k+1} \sim 0.63r_{{\rm s},k}$. The satellite system formed from a disk with $M^0_{\rm disk} = 0.003M_{\rm c}$ resembles

Galilean satellites. Note that the satellite system of Uranus resembles the satellite system of Jupiter (Figs. 1), and the satellite system of Saturn also resembles them, though Titan may be exceptionally large.

While the satellites are formed from the disk, the disk mass diminishes and satellite formed from the disk becomes smaller. If the satellites are much smaller than the satellites in our simulations, disk-satellite interaction would be much smaller and they would not able to wipe the disk mass up to 2:1 resonance. Thus, the masses of satellites and their intervals would become smaller as the disk mass diminishes. This tendency is consistent with the observed tendency that the inner satellites has the smaller mass. This may account for the existence and its distribution of small satellites in the inner part of satellite system, and the ring of Saturn may be a remnant of the proto-satellite disk. More investigations are needed.

A disk with mass $M^0_{\rm disk} \sim 0.003 M_{\rm c}$ could form a satellite system with number and satellite mass similar to Galilean satellites. In the case of Jupiter, the mass $0.003 M_{\rm c}$ is about the Earth mass $1 M_{\oplus}$. In the final stage of solar system formation, it is considered that protoplanets are formed from the swarm of planetesimals. In the theory of oligarchic growth, protoplanets of $\sim 7 M_{\oplus}$ would be formed with orbital separation ~ 2 AU in the region of $r \sim 7$ AU (Ida & Kokubo 1998). Considering that two of them grows to Jupiter ($R_{\rm J} \sim 5.2$ AU) and Saturn ($R_{\rm S} \sim 9.5$ AU) by the onset of gas accretion, several protoplanets which failed in gas accretion would remain nearby. Thus, it may be possible that a grazing collision of a protoplanet with mass $\sim 7 M_{\oplus}$ with a giant planet Jupiter makes a disk with $M_{\oplus}$.

In this paper, we investigated the satellite formation from a disk which is radially compact. We consider the case that the initial disk is radially spreaded to a scale of a present regular satellite system. In this case, satellite would be formed in a similar way to a planetary formation. A relatively large object would grow in a runaway manner, until the materials in a collisional zone accumulate into a single body. The intervals between such proto-satellites depends on a time scale of accretion. If a time scale of accretion is short comparing with the time scale of orbital repulsion, the interval Δr is (Lissauer

1987) $\Delta r \sim 3.5 r_{\rm H}$. If the time scale of accretion is slow, its factor increases up to 5-10 (Kokubo & Ida 1995). In a case of satellite accretion, a particles occupies much larger fraction of its Hill's sphere than a case of planetary accretion, so that accretion would be fast. In Figs. 1, we have shown the range within 5 $r_{\rm H}$ of each satellite by a horizontal bar. As have shown in Figs. 1, present intervals of satellites are much larger than $3.5 r_{\rm H}$. From a disk with the scale of present regular satellite system, much more small proto-satellites would be formed. In this case, long term instability (Chambers, Whetherill, & Boss 1996) and giant impacts between proto-satellite may leads to a satellite system similar to present ones.

6.3. Future Works

The evolution of the massive debris disk is rather simple, since it is mainly regulated by the viscous spreading of the disk. However, as the disk becomes less massive, the time scale of viscous spreading increases, and tidal orbital evolution, which we do not take into account in the present paper may also be important. To explore the evolution of less massive disks, which would result in the multiple satellite system, coupled orbital evolutions due to disk-satellite interaction and tidal interaction between the satellite and a central planet must be investigated. Also, the stability of the multiple satellite system must be investigated, including the effect of tide from the central planet (Canup, Levison, & Stewart 1999).

I am grateful to Assistant Professor S. Ida for his much helpful advise and critical readings. I thank Dr. H. Tanaka for valuable discussions. My numerical calculations were performed by special purpose hardware Grape-5 system MUV at Astronomical Data Analysis Center, National Astronomical Observatory. I thank all the members of Department of Earth and Planetary Sciences, and Astronomical Data Analysis Center. I thank Takenaka Scholarship Association for generous supports. Finally, I thank my family.

REFERENCES

Araki, S. & Tremaine, S. 1986. The dynamics of dense particle disks. *Icarus* **65**, 83

Binney, J., & Tremaine, S. 1987. *Galactic dynamics* (Princeton, NJ, Princeton University Press).

Canup, R. M., Levison, H. F., & Stewart, G. R. 1999. Evolution of a terrestrial multiple-moon system. *AJ* **117**, 603

Cameron, A. G. W. & Ward, W. R. 1976. The origin of the moon. *Lunar Sci. Abs.* **7**, 120

Chambers, J. E., Wetherill, G. W., & Boss, A. P. 1996. The Stability of Multi-Planet Systems. *Icarus* **119**, 261

Daisaka, H. & Ida, S. 1999. Spatial structure and coherent motion in dense planetary rings induced by self-gravitational instability. *Earth and Planet and Space* **51**, 1195

Daisaka, H., Tanaka, H., & Ida, S. 2001. Viscosity in a dense planetary ring with self-gravitating particles. *Icarus*, in press.

Goldreich, P., & Tremaine, S. 1978. The velocity dispersion in Saturn's rings. *Icarus* **34**, 227

Goldreich, P., & Tremaine, S. 1979. The excitation of density waves at the Lindbrad and corotation resonances by an external potential. *ApJ* **233**, 857

Goldreich, P. & Tremaine, S. 1980. The disk-satellite interactions. *ApJ* **241**, 425

Goldreich, P. & Tremaine, S. 1982. The dynamics of planetary rings. *Ann. Rev. Astron. Astrophys.* **20**, 249

Hartmann, W. K. & Davis, D. R. 1975. Satellite-sized planetesimals and lunar origin. *Icarus* **24**, 504

Hasegawa, M., & Nakazawa, K. 1990. Distant encounter between Keplerian particles. *Astron. Astrophys.* **227**, 619

Ida, S., & Nakazawa, K. 1989. Collisional probability of planetesimals revolving in the solar gravitating field III. *Astron. Astrophys.* **224**, 303

Ida, S. 1990. Stirring and dynamical friction rates of planetesimals in the solar gravitational field. *Icarus* **88**, 129

Ida, S., Canup, R. M., & Stewart, G. R. 1997. Lunar accretion from an impact-generated disk. *Nature* **389**, 353

Ida, S., & Kokubo, E. 1998. Oligarchic growth of protoplanets. *Icarus* **131**, 171

Kawai, A., Fukushige, T., Makino, J., & Taiji, M. 2000. GRAPE-5: A special-purpose computer for N-body simulation. *PASJ* **52**, 659

Kokubo. E., Ida, S. 1995 Orbital Evolution of Protoplanets Embedded in a Swarm of Planetesimals. *icarus* **114**, 247

Kokubo, E., Ida, S., & Makino J. 2000. Evolution of a circumterrestrial disk and formation of a single moon. *Icarus* **148**, 419

Nakazawa, K., Ida, S., & Nakagawa, Y. 1989. Collisional probability of planetesimals revolving in the solar gravitational field I. Basic equation. *Astron. Astrophys* **220**, 293

Larson, R.B. 1984. Gravitational torques and star formation. *MNRAS* **206**, 197

Lin, D.N.C., & Papaloizou, J.C. 1993. On the tidal interaction between protosteller disks and companions. in *Protostars and Planets III* , ed. Levy, E.H. & Lunine J.I. (Univ. of Arizona Press), 749

Lin, D.N.C., & Pringle, J.E. 1987. A viscosity prescription for a self-gravitating accretion disc *MNRAS* **225**, 607

Lunine J.I., & Tittemore W.C. 1993. Origins of outer-planet satellites. in *Protostars and Planets III* , ed. Levy, E.H. & Lunine J.I. (Univ. of Arizona Press), 1149

Lynden-Bell, D., & Kalnajs, A. J. 1972. On the generating mechanism of spiral structure. *MNRAS* **157**, 1

Lynden-bell, D., and Pringle, J.E. 1974. The evolution of viscous discs and the origin of the nebular variables. *MNRAS* **168**, 603

Makino, J., & Aarseth, S.J. 1992. On a Hermite integrator with Ahmad-Cohen scheme for gravitational many-body problems. *PASJ* **44**, 141

Makino, J., Taiji, M., Ebisuzaki, T., & Sugimoto, D. 1997. GRAPE-4: A massively parallel special-purpose computer for collisional N-body simulations. *ApJ* **480**, 432

Peale, S.J., 1986. Orbital resonances, unusual configurations and exotic rotation states among planetary satellites, in *Satellite*, ed. Burns, J.A., and Matthews, M.S. (Univ. of Arizona Press), 159

Petit, J.-M., and Hénon M., 1984. A numerical simulation of planetary rings. I. Binary encounters. *Astron. Astrophys.* **173**, 389

Petit, J.-M., and Hénon M. 1986. Satellite encounters. *Icarus* **66**, 536

Petit, J.-M., and Hénon M. 1988. A numerical simulation of planetary rings. III. Mass segregation, ring confinement, and gap formation. *Astron. Astrophys* **199**, 343

Pollack, J.B., Lunine, J.I. & Tittemore, W.C. 1991. Origin of the Uranian satellites. in *Uranus* , ed. Bergstralh, J.T., Miner, E.D., & Matthews, M.S. (Univ. of Arizona Press), 469

Pringle, J.E. 1981. Accretion discs in astrophysics. *Ann. Rev. Astron. Astrophys.*, 19, 137

Lissauer, J. J. 1987. Timescales for Planetary Accretion and the Structure of the Protoplanetary Disk. *Icarus* **1987**, 249

Lissauer, J. J. 1995. Urey prize lecture: On the diversity of diversity of plausible planetary systems. *Icarus* **114**, 217

Richardson, D. C. 1994. Tree code simulations of planetary rings. *MNRAS* **269**, 493

Salo, H. 1995. Simulations of dense planetary rings. III. Self-gravitating identical particles. *Icarus* **117**, 287

Stevenson, D.J., Harris, A.W., and Lunine, J.I. 1986. Origins of satellites, in *Satellite*, ed. Burns, J.A., and Matthews, M.S. (Univ. of Arizona Press), 39

Takdea, T., & Ida S. 2001. Angular momentum transfer in a protolunar disk. *ApJ* **540**, 514

Toomre, A. 1964. On the gravitational stability of a disk of stars. *ApJ* **139**, 1217

Ward W.R., & Cameron A.G.W. 1978. Disc evolution within the Roche limit. *Proc. Lunar Planet. Sci. Conf., Abs.* **IX**, 1205

Wisdom, J., & Tremaine, S. 1988. Local simulations of planetary rings. *AJ* **95**, 925

This preprint was prepared with the AAS LaTeX macros v5.0.